



Chinese Pharmaceutical Association  
Institute of Materia Medica, Chinese Academy of Medical Sciences

Acta Pharmaceutica Sinica B

[www.elsevier.com/locate/apsb](http://www.elsevier.com/locate/apsb)  
[www.sciencedirect.com](http://www.sciencedirect.com)



ORIGINAL ARTICLE

# Structure-based design and optimization lead to the identification of novel dihydrothiopyrano [3,2-*d*]pyrimidine derivatives as potent HIV-1 inhibitors against drug-resistant variants



Zhao Wang<sup>a,c,d,†</sup>, Heng Zhang<sup>a,†</sup>, Zhen Gao<sup>a</sup>, Zihao Sang<sup>a</sup>, Erik De Clercq<sup>b</sup>, Christophe Pannecouque<sup>b,\*</sup>, Dongwei Kang<sup>a,c,\*</sup>, Peng Zhan<sup>a,c,\*</sup>, Xinyong Liu<sup>a,c,\*</sup>

<sup>a</sup>Department of Medicinal Chemistry, Key Laboratory of Chemical Biology (Ministry of Education), School of Pharmaceutical Sciences, Cheeloo College of Medicine, Shandong University, Jinan 250012, China

<sup>b</sup>Rega Institute for Medical Research, Laboratory of Virology and Chemotherapy, K.U. Leuven, Leuven B-3000, Belgium

<sup>c</sup>China-Belgium Collaborative Research Center for Innovative Antiviral Drugs of Shandong Province, Jinan 250012, China

<sup>d</sup>Suzhou Research Institute, Shandong University, Suzhou 215123, China

Received 1 August 2023; received in revised form 3 November 2023; accepted 14 November 2023

## KEY WORDS

HIV-1;  
Reverse transcriptase;  
Dihydrothiopyrano[3,2-*d*]  
pyrimidine;  
Antiviral agent

**Abstract** With our continuous endeavors in seeking potent anti-HIV-1 agents, we reported here the discovery, biological characterization, and druggability evaluation of a class of nonnucleoside reverse transcriptase inhibitors. To fully explore the chemical space of the NNRTI-binding pocket, novel series of dihydrothiopyrano [3,2-*d*]pyrimidines were developed by employing the structure-based design strategy. Most of the derivatives were endowed with prominent antiviral activities against HIV-1 wild-type and resistant strains at nanomolar levels. Among them, compound **23h** featuring the aminopiperidine moiety was identified as the most potent inhibitor, with EC<sub>50</sub> values ranging from 3.43 to 21.4 nmol/L. Especially, for the challenging double-mutants F227L + V106A and K103N + Y181C, **23h** exhibited 2.3- to 14.5-fold more potent activity than the first-line drugs efavirenz and etravirine. Besides, the resistance profiles of **23h** achieved remarkable improvement compared to efavirenz and etravirine. The binding

\*Corresponding authors.

E-mail addresses: [christophe.pannecouque@rega.kuleuven.be](mailto:christophe.pannecouque@rega.kuleuven.be) (Christophe Pannecouque), [kangdongwei@sdu.edu.cn](mailto:kangdongwei@sdu.edu.cn) (Dongwei Kang), [zhanpeng1982@sdu.edu.cn](mailto:zhanpeng1982@sdu.edu.cn) (Peng Zhan), [xinyongl@sdu.edu.cn](mailto:xinyongl@sdu.edu.cn) (Xinyong Liu).

†These authors made equal contributions to this work.

Peer review under the responsibility of Chinese Pharmaceutical Association and Institute of Materia Medica, Chinese Academy of Medical Sciences.

<https://doi.org/10.1016/j.apsb.2023.11.023>

2211-3835 © 2024 The Authors. Published by Elsevier B.V. on behalf of Chinese Pharmaceutical Association and Institute of Materia Medica, Chinese Academy of Medical Sciences. This is an open access article under the CC BY-NC-ND license (<http://creativecommons.org/licenses/by-nc-nd/4.0/>).

target of **23h** was further confirmed to be HIV-1 reverse transcriptase. Molecular modeling studies were also performed to elucidate the biological evaluation results and give guidance for the optimization campaign. Furthermore, no apparent inhibition of the major CYP450 enzymes and hERG channel was observed for **23h**. Most importantly, **23h** was characterized by good pharmacokinetic properties and excellent safety *in vivo*. Collectively, **23h** holds great promise as a potential candidate for its effective antiviral efficacy and favorable drug-like profiles.

© 2024 The Authors. Published by Elsevier B.V. on behalf of Chinese Pharmaceutical Association and Institute of Materia Medica, Chinese Academy of Medical Sciences. This is an open access article under the CC BY-NC-ND license (<http://creativecommons.org/licenses/by-nc-nd/4.0/>).

## 1. Introduction

Human immunodeficiency virus-1 (HIV-1) is the major pathogen of acquired immune deficiency syndrome (AIDS), which remains a serious epidemic disease threatening global public health<sup>1,2</sup>. Benefit from the development of antiviral agents for different stages of the HIV-1 replication cycle, the application of combination antiretroviral therapy (cART) has successfully transformed AIDS from a fatal disease to a controllable chronic disease<sup>3</sup>. Reverse transcriptase (RT) is an attractive HIV-1 therapeutic target due to the validated biochemical mechanism and abundant structural information, which plays a unique role in transcribing ssRNA into dsDNA<sup>4,5</sup>.

HIV-1 RT inhibitors can be divided into nucleoside RT inhibitors (NRTIs) and nonnucleoside RT inhibitors (NNRTIs) based on distinct binding sites and mechanisms of action<sup>6</sup>. NRTIs are competitively integrated into the processing DNA to produce chain termination by acting as natural substrate analogues. NNRTIs occupy the induced allosteric site, called the NNRTI-binding pocket (NNIBP), leading to conformational changes in the active site and inhibition of catalytic activity<sup>7,8</sup>. NNRTIs have become an increasingly essential component of cART for their robust potency, high specificity, and lack of mitochondrial toxicity, and they are available in the first two-drug single-tablet regimen Juluca<sup>®</sup> (rilpivirine + dolutegravir)<sup>9</sup> and the first long-acting injectable formulation Cabenuva<sup>®</sup> (rilpivirine + cabotegravir)<sup>10</sup> for maintenance of virological suppression<sup>11</sup>.

Diarylpyrimidine (DAPY) derivatives characterized by a central pyrimidine ring and two aromatic wings have attracted widespread attention as the most successful class of HIV-1 NNRTIs<sup>12,13</sup>. The FDA-approved drugs etravirine (**1**, ETR) and rilpivirine (**2**, RPV) possess extraordinarily potent antiviral activities against various resistant strains selected by the earlier NNRTIs and are developed as once-daily oral tablets (Fig. 1)<sup>7,12</sup>. Another promising drug dapivirine (**3**, DPV) is later applied as a

vaginal microbicide due to its different oral bioavailability and long half-life<sup>14</sup>. A vaginal ring containing DPV was approved by the European Medicines Agency (EMA) in 2020 as an effective pre-exposure prophylaxis (PrEP) agent for HIV-1 prevention<sup>15</sup>. Nevertheless, new mutations with decreased susceptibility to ETR or RPV and aggravated cross-resistance continue to emerge in clinical treatment due to the inherent high mutation rate of viral genetic material, for instance, L100I for ETR and Y188L for RPV, especially the most challenging double-mutants F227L + V106A and K103N + Y181C<sup>16,17</sup>. Moreover, both ETR and RPV suffer from poor water solubility (Sol. < 1 µg/mL) and pharmacokinetic (PK) properties on account of excessive lipophilic rings in the rigid structure, and there are no accurately measured oral bioavailability data<sup>18</sup>. Consequently, unremitting efforts are still required to focus on extensive structural optimizations of DAPY derivatives to seek novel inhibitors with higher drug-resistance profiles and good pharmacological properties.

As is well known, classical structure-based drug design strategies usually focus on the systematic modifications of specific molecular structures to explore the accessible chemical space and enhance the affinity with the target protein<sup>19,20</sup>. According to the recent advances in crystallographic studies, all DAPY derivatives share a horseshoe-shaped binding conformation and contain four pivotal pharmacophoric features<sup>21,22</sup>. Therefore, in the present work, extensive molecular elaborations have been conducted based on the “four-point pharmacophore” model by investigating the potential binding sites of tolerant region I, tolerant region II, hydrophobic channel, and hydrogen bonding interaction domain to discover new HIV-1 inhibitors with elevated biological activity and favorable druggability profiles (Fig. 2).

(i) Tolerant region II: The central scaffold of DAPYs is located in the tolerant region II (*i.e.*, entrance channel) composed of amino acid residues Leu100, Glu138, and Val179. During lead optimization, the  $Fsp^3$  parameter was introduced as a novel metric to assess drug-like properties by quantifying the carbon saturation and spatial complexity of molecules. It represents the fraction of  $sp^3$  hybridized carbon atoms, calculated as the ratio of the number of  $sp^3$  hybridized carbon atoms to the total carbon count, which has been proven to be positively correlated with the clinical success rate<sup>23,24</sup>. However, ETR and RPV have low  $Fsp^3$  values because of the introduction of three aromatic rings. Consequently, the saturated dihydrothiopyrano ring with high  $Fsp^3$  content and large molecular volume was fused to the central scaffold by cyclizing the pyrimidine ring, in the hope that the newly introduced non-planar structure could reduce the crystal packing of aromatic molecules and fully occupy the

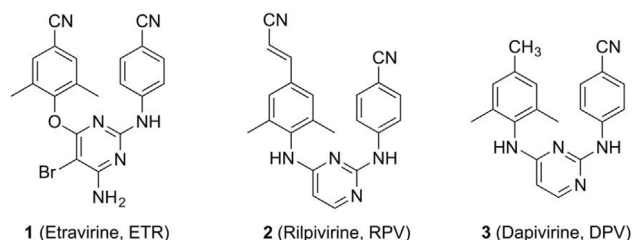


**Figure 1** Chemical structures of the approved drugs (ETR, RPV, and DPV).

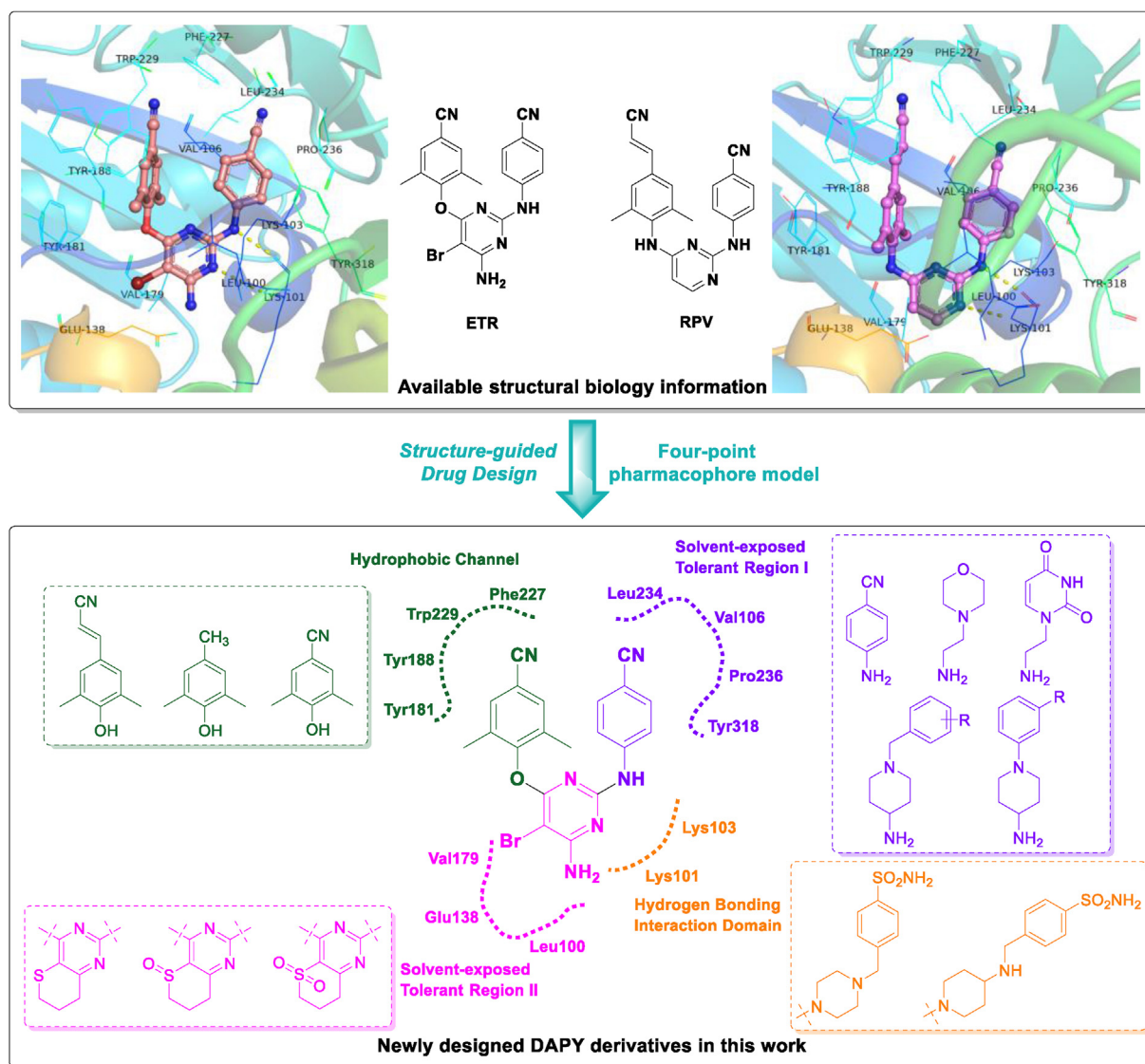


**Figure 2** Multidimensional optimization of diarylpyrimidine derivatives based on the “four-point pharmacophore” model.

binding pocket. Besides, the S atom possesses a comparable atomic radius ( $r_s = 104$  pm) and lone pair electron as the Br atom ( $r_{Br} = 114$  pm), which may contribute to the formation of non-polar interaction with Glu138 and electrostatic interaction with Leu100 and Val179.

- (ii) Hydrogen bonding interaction domain: The NH linker and the pyrimidine 1'-N atom establish key dual hydrogen bonds with the main chain of Lys101. So the piperazine and amino-piperidine substituted with benzylsulfonamide directly connected to the central scaffold *via* a carbon–nitrogen bond were introduced to replace the NH linker to determine the necessity of dual hydrogen bonds for the maintenance of activity.
- (iii) Hydrophobic channel: The left-wing 2,4,6-trisubstituted phenyl moiety of DAPYs occupies the hydrophobic channel consisting of aromatic residues Tyr181, Phe227, and Trp229. Therefore, three preferred substituents (cyano, cyanovinyl, and methyl) derived from the approved drugs (ETR, RPV, and

DPV) were installed on the left-wing to yield effective  $\pi$ – $\pi$  stacking interactions.

- (iv) Tolerant region I: The right-wing *p*-cyanoaniline fragment of DAPYs points to a broad plastic “groove” surrounded by residues Val106, Leu234, Pro236, and Tyr318, termed as the solvent-exposed tolerant region I (*i.e.*, the Pro236 hairpin loop). Recently, a novel class of catechol diether derivatives was disclosed as potent NNRTIs with robust antiviral activities at picomolar levels and favorable physico-chemical properties (Fig. 3), exemplified by compounds **4** (JLJ494,  $EC_{50} = 0.055$  nmol/L) and **5** (JLJ636,  $EC_{50} = 1.9$  nmol/L)<sup>25,26</sup>. Moreover, the crystallographic overlay of DAPYs and catechol diethers indicated that the ethyluracil moiety is oriented towards the tolerant region I. Furthermore, morpholine as a frequently used heterocycle for medicinal chemistry is employed in numerous bioactive molecules, mainly due to its advantageous contribution to the biological and metabolic properties<sup>27</sup>. Besides, in our

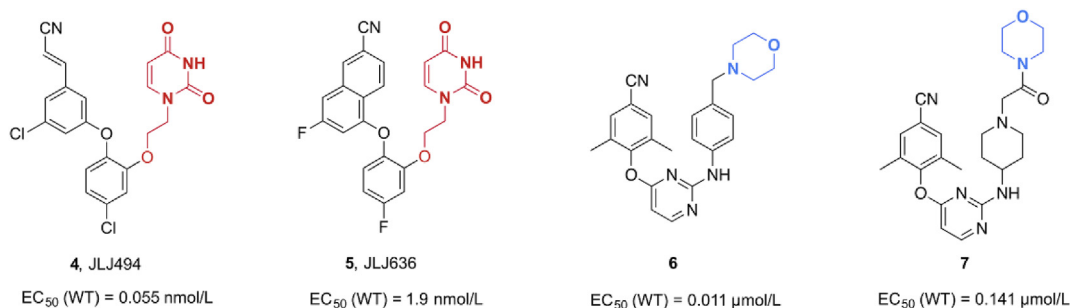


**Figure 3** Chemical structures of the representative NNRTI lead compounds containing uracil (catechol diether derivatives **4** and **5**) or morpholine (diarylpyrimidine derivatives **6** and **7**).

previous work, compounds **6** (EC<sub>50</sub> = 0.011 μmol/L) and **7** (EC<sub>50</sub> = 0.141 μmol/L) with moderate inhibitory potency were discovered by introducing morpholine into the tolerant region I (Fig. 3)<sup>28,29</sup>. Therefore, uracil and morpholine with a terminal ethylamino group were applied to the right-wing portion as a solvent-friendly fragment to investigate the suitability of tolerant region I. In addition, considering that the flexible piperidine ring could adapt well to the variations of the binding site caused by residue mutations<sup>30,31</sup>, the *p*-cyanoaniline was replaced by the privileged piperidine-linked benzyl or phenyl motif to improve the drug resistance profiles.

The energy required to shift from the lowest energy preferred conformation to the pharmacophoric conformation adopted by the ligand to bind to the protein binding site can be compensated by the binding energy released by drug–target interactions<sup>32,33</sup>. Therefore, the conformational difference between the preferred conformation and the pharmacophoric conformation directly affects the binding affinity of the drug to the target<sup>34</sup>. Notably, the lowest energy preferred conformation of novel derivatives with distinct scaffolds were found to superimpose well with their pharmacophoric conformation in the RT allosteric binding site, preliminarily validating the rationality of the design idea based on the four-point pharmacophore model (Fig. 4).

Herein, we described the rational design and multidimensional optimization of novel dihydrothiopyrano [3,2-*d*]pyrimidine derivatives as potent HIV-1 inhibitors. Besides, the preliminary SARs were discussed in detail to guide further work. More importantly, the biological characterization and druggability evaluation of the most promising compound **23h** were performed to confirm the feasibility of **23h** as a potential drug candidate.

## 2. Results and discussion

### 2.1. Chemistry

The newly designed derivatives were prepared *via* four concise synthetic routes<sup>35–37</sup>. As shown in Scheme 1, methyl 2-mercaptoacetate (**8**) was reacted with methyl 4-chlorobutanoate to afford intermediate **9**. Then the cyclization of **9** with NaH generated **10**, which was condensed with *S*-methylthiuronium sulfate to produce **11**. Next, **11** was hydrolyzed with HOAc to provide **12**, followed by chlorination of the hydroxyl group with POCl<sub>3</sub> to give the key intermediate **13**. The nucleophilic addition of **13** with different phenols yielded the corresponding intermediates **14a–c**. Intermediates **14a** or **14b** underwent the palladium catalyzed Buchwald–Hartwig reaction with BINAP and Pd<sub>2</sub>(dba)<sub>3</sub> to provide the final products **15a** and **15b**. The oxidative products **16a** and **16b** were prepared by treating **15a** with *m*-CPBA at –78 °C or room temperature.

As depicted in Scheme 2, treatment of **14a** with 1-Boc-piperazine or 4-Boc-aminopiperidine in the presence of K<sub>2</sub>CO<sub>3</sub> at 120 °C gave the intermediates **17a** or **17b**. Removal of the Boc group provided the intermediates **18a** or **18b**, which then resulted in the target compounds **19a** and **19b** after nucleophilic substitution with 4-(bromomethyl)benzenesulfonamide. In addition, the intermediates **14a–c** were converted into the target compounds **20a–d** by reacting with 1-(2-aminoethyl)pyrimidine-2,4(1*H*,3*H*)-dione or 2-morpholinoethan-1-amine.

As illustrated in Scheme 3, **14a–c** were reacted with 4-amino-1-Boc-piperidine in the presence of K<sub>2</sub>CO<sub>3</sub> at 100 °C to provide the intermediates **21a–c**, which afforded the key analogues **22a–c** after removal of the Boc protecting group. Subsequently, the target compounds **23a–i** were obtained from the

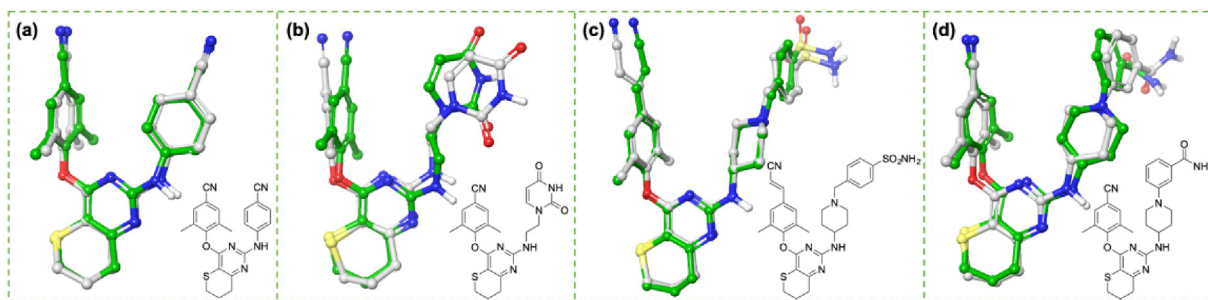
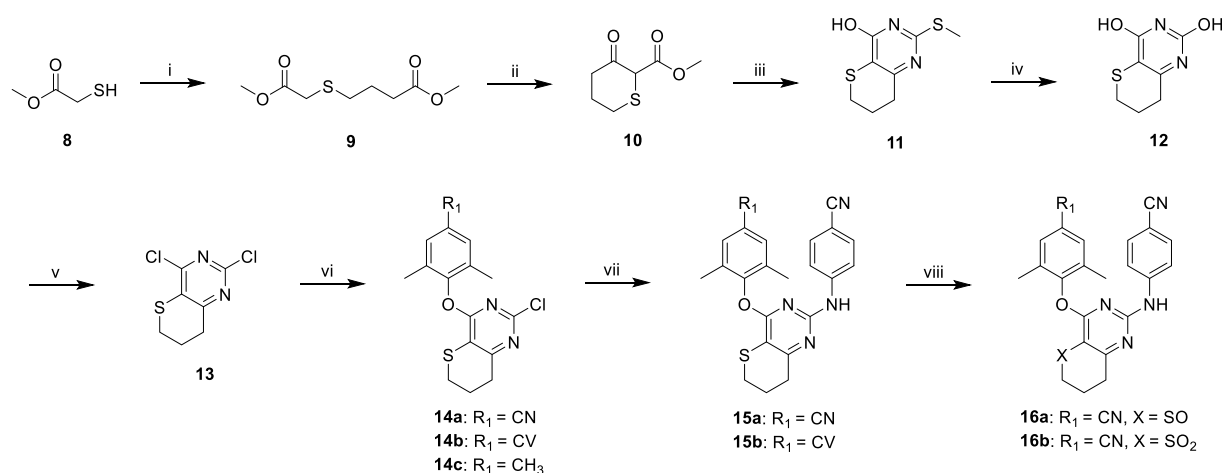
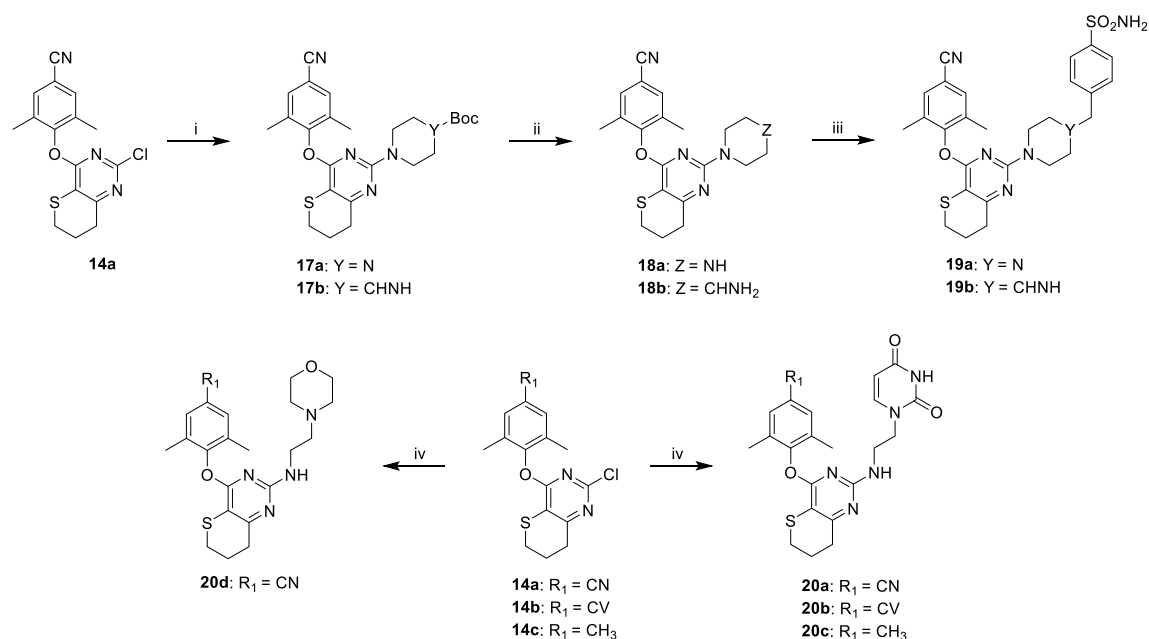


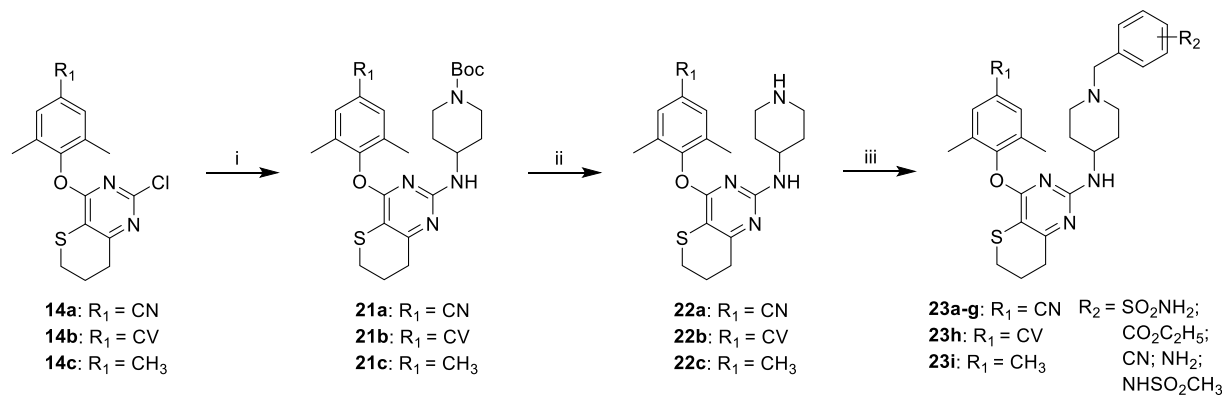
**Figure 4** Overlay of the lowest energy preferred conformation (white) and the pharmacophoric conformation (green) of the representative molecules with distinct scaffolds. Predicted binding mode of ligands with the HIV-1 WT RT (PDB code: 6CON).



**Scheme 1** Reagents and conditions: (i) methyl 4-chlorobutanoate, MeONa, KI, MeOH, 70 °C; (ii) NaH, THF, 0 °C to r.t.; (iii) *S*-methylthiuronium sulfate, KOH, MeOH, r.t.; (iv) HOAc, H<sub>2</sub>O, 110 °C; (v) POCl<sub>3</sub>, *N,N*-dimethylaniline, 110 °C; (vi) K<sub>2</sub>CO<sub>3</sub>, DMF, r.t.; (vii) 4-aminobenzonitrile, BINAP, Pd<sub>2</sub>(dba)<sub>3</sub>, Cs<sub>2</sub>CO<sub>3</sub>, 1,4-dioxane, 100 °C; (viii) *m*-CPBA, DCM, -78 °C or r.t.



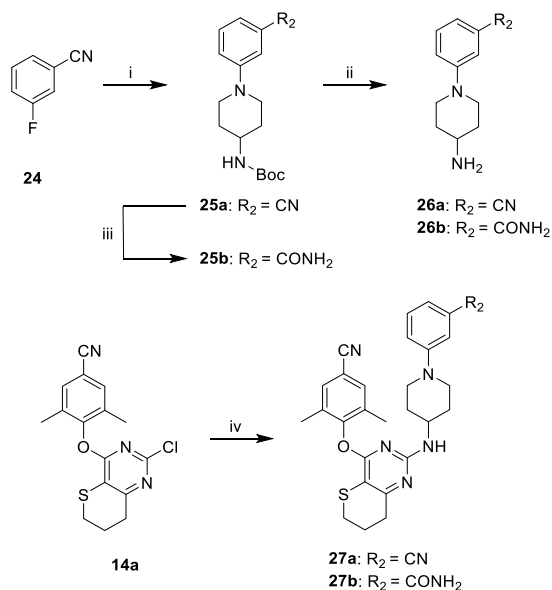
**Scheme 2** Reagents and conditions: (i) K<sub>2</sub>CO<sub>3</sub>, DMF, 100 °C; (ii) TFA, DCM, r.t.; (iii) 4-(bromomethyl)benzenesulfonamide, K<sub>2</sub>CO<sub>3</sub>, DMF, r.t.; (iv) DIEA, NMP, 120 °C.



**Scheme 3** Reagents and conditions: (i) K<sub>2</sub>CO<sub>3</sub>, DMF, 100 °C; (ii) TFA, DCM, r.t.; (iii) K<sub>2</sub>CO<sub>3</sub>, DMF, r.t.

nucleophilic reaction of **22a–c** and various benzyl chlorides/bromides.

As shown in Scheme 4, treatment of 3-fluorobenzonitrile (**24**) with *tert*-butyl piperidin-4-ylcarbamate furnished the cyano intermediate **25a** and hydrolysis of **25a** under NaOH and H<sub>2</sub>O<sub>2</sub> generated the amide intermediate **25b**, followed by removing the Boc group to give intermediates **26a** and **26b**. Finally, **14a** was



**Scheme 4** Reagents and conditions: (i) *tert*-butyl piperidin-4-ylcarbamate, K<sub>2</sub>CO<sub>3</sub>, DMF, 120 °C; (ii) TFA, DCM, r.t.; (iii) NaOH, H<sub>2</sub>O<sub>2</sub>, EtOH, 50 °C; (iv) 3-(4-aminopiperidin-1-yl)benzonitrile or 3-(4-aminopiperidin-1-yl)benzamide, BINAP, Pd<sub>2</sub>(dba)<sub>3</sub>, Cs<sub>2</sub>CO<sub>3</sub>, 1,4-dioxane, N<sub>2</sub>, 100 °C.

coupled with the above intermediates **26a** or **26b** via the Buchwald–Hartwig reaction to prepare the target compounds **27a** and **27b**.

## 2.2. Anti-HIV activity evaluation

All the target compounds were first screened for their anti-HIV activities against the WT (IIIB) and double-mutant K103N + Y181C (RES056) HIV-1 strains. Partially representative compounds with prominent activities were further evaluated for their inhibitory potency against a panel of clinically relevant HIV-1 variants carrying single-mutations L100I, K103N, E138K, Y181C, Y188L, or double-mutations F227L + V106A. Biological evaluation results are presented as EC<sub>50</sub> (50% effective concentration of test compound) and CC<sub>50</sub> (50% cytotoxic concentration of test compound) values.

As illustrated in Tables 1–3, most compounds displayed excellent potency against IIIB strain in the single-digit to double-digit nanomolar ranges (EC<sub>50</sub> = 1.44–20.0 nmol/L). Among them, compound **16b** was the most active IIIB inhibitor with an EC<sub>50</sub> of 1.44 nmol/L, being slightly superior to ETR (EC<sub>50</sub> = 2.81 nmol/L) and EFV (EC<sub>50</sub> = 2.67 nmol/L), and comparable to RPV (EC<sub>50</sub> = 1.00 nmol/L). As for the most challenging double-mutant variant RES056, compounds with high potency toward the IIIB strain were also found to be effective at inhibiting the RES056 strain (EC<sub>50</sub> = 15.2–445 nmol/L). Five compounds (**15a**, **15b**, **16b**, **23h**, and **27b**) yielded greater potency than EFV (EC<sub>50</sub> = 114 nmol/L), with EC<sub>50</sub> values of 15.2–85.3 nmol/L. In particular, compound **23h** (EC<sub>50</sub> = 15.2 nmol/L) was identified as the most powerful inhibitor against RES056 strain, being up to 2.3- and 7.5-fold greater than ETR (EC<sub>50</sub> = 35.2 nmol/L) and EFV (EC<sub>50</sub> = 114 nmol/L), but slightly weaker than RPV (EC<sub>50</sub> = 10.7 nmol/L). Besides, most of the novel compounds had decreased cytotoxicity (CC<sub>50</sub> = 3.07–284 μmol/L) compared to ETR (CC<sub>50</sub> = 2.20 μmol/L) and RPV (CC<sub>50</sub> = 3.98 μmol/L),

**Table 1** Anti-HIV-1 (IIIB and RES056) activity and cytotoxicity of **15a–b** and **16a–b** in MT-4 cells.

Compd.	R <sub>1</sub>	X	EC <sub>50</sub> (nmol/L) <sup>a</sup>		CC <sub>50</sub> (μmol/L) <sup>b</sup>
			IIIB	RES056	
			<b>15a-b</b>	<b>16a-b</b>	
<b>15a</b>	CN	S	3.38 ± 3.17	85.3 ± 54.3	4.53 ± 0.72
<b>15b</b>	CV	S	3.18 ± 1.21	23.5 ± 14.7	4.89 ± 0.62
<b>16a</b>	CN	SO	7.99 ± 0.95	445 ± 95.7	≥19.7
<b>16b</b>	CN	SO <sub>2</sub>	1.44 ± 0.17	49.1 ± 14.0	18.7 ± 8.01
NVP	—	—	118 ± 66.9	2221 ± 736	>15.0
EFV	—	—	2.67 ± 1.73	114 ± 55.6	>6.34
ETR	—	—	2.81 ± 0.47	35.2 ± 19.7	2.20 ± 0.015
RPV	—	—	1.00 ± 0.27	10.7 ± 7.96	3.98

<sup>a</sup>EC<sub>50</sub>: concentration of compound required to achieve 50% protection of MT-4 cell cultures against HIV-1-induced cytopathicity, as determined by the MTT method.

<sup>b</sup>CC<sub>50</sub>: concentration required to reduce the viability of mock-infected cell cultures by 50%, as determined by the MTT method.

contributing to the higher SI values and reflecting their sufficient safety profiles at the *in vitro* cellular level.

Based on the antiviral evaluation (IIIB and RES056 strains) results, preliminary SAR of these novel derivatives could be delineated: Firstly, with ETR as the lead compound, a non-planar dihydrothiopyrano moiety was introduced into the central ring, with the aim of fully occupying the tolerant region II to improve antiviral activities and physicochemical properties. As depicted in Table 1, compounds **15a–b** and **16a–b** were able to potently inhibit the HIV-1 IIIB ( $EC_{50} = 1.44–7.99$  nmol/L) and RES056 strains ( $EC_{50} = 23.5–445$  nmol/L), while exhibiting reduced cytotoxicity ( $CC_{50} \geq 4.53$   $\mu$ mol/L) compared to ETR and RPV. Analysis of SAR revealed that the nature of substituents at the  $R_1$  or X position had a significant influence on the antiviral activity. Pairwise comparison of compounds **15a** and **15b** indicated that the cyanovinyl group at the  $R_1$  position favored the potency over the cyano group, due to enhanced  $\pi$ -stacking interaction with the hydrophobic channel. Sulfonation at the X position resulted in a more potent inhibitor **16b**, but the introduction of the sulfoxide group afforded **16a** with sharply reduced activity. Thus, the established SAR confirmed that the newly introduced dihydrothiopyrano moiety fits well in the tolerant region II to improve binding affinity.

In continuation of our efforts, we set out to introduce distinct moieties derived from other classes of NNRTIs at the right-wing and linker to replace the *p*-cyanoaniline fragment, affording derivatives **19a–b** and **20a–d** based on the molecular hybridization strategy. However, as shown in Table 2, all compounds showed very weak or even loss of activity toward IIIB and RES056 strains. Directly attaching the central scaffold to piperazine and piperidine *via* a carbon-nitrogen bond to remove the NH linker resulted in the discovery of **19a** and **19b** with lost potency. Thus, the critical double hydrogen bonds involved in

the right imino linker are necessary to maintain the binding force, which also suggests that the inherent conformational flexibility ensures favorable resistance profiles of DAPY NNRTIs. Moreover, to further investigate the tolerant region I, **20a–d** were designed by molecular hybridization of DAPYs with catechol diethers and morpholine derivatives. Regrettably, replacement of the *p*-cyanoaniline moiety of **15a** with ethylamino-containing uracil and morpholine yielded **20a** and **20d** with sharply decreased activities against WT and RES056 strains, probably because the uracil and morpholine were too flexible to fully occupy the tolerant region I. The potency order of **20a–c** was as follows: **20b** (–CV) > **20a** (–CN) > **20c** (–CH<sub>3</sub>), indicating that cyanovinyl and cyano are more favorable than methyl for binding affinity.

In an effort to fully explore the SAR of these dihydrothiopyrano[3,2-*d*]pyrimidines, we attempted to replace the *p*-cyanoaniline group with privileged piperidine-linked benzyl or phenyl moieties to improve resistance profiles, considering that the piperidine ring can adapt to the changed binding pockets through flexible conformation. Meanwhile, structurally diverse substituents were introduced to the terminal benzene ring, to reach into the tolerant region I and form additional interactions. As shown in Table 3, most of compounds **23a–i** and **27a–b** exhibited single-digit nanomolar inhibitory activity against the IIIB strain and maintained moderate potency against the RES056 strain. Further investigation of SAR revealed that the  $R_2$  substituents on the phenyl group significantly affected the anti-HIV-1 potency. The comparison between compounds **23a–c** indicated that the antiviral activity was dependent on the  $R_2$  substitution position of the benzene moiety and that the *para*-substitution was preferred over the *meta*- and *ortho*-substitution. Besides, the compounds with *para*-substituted phenyl were in the following order of potency:

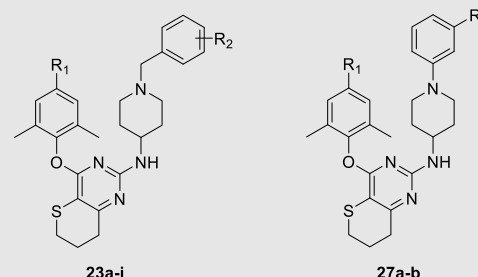
**Table 2** Anti-HIV-1 (IIIB and RES056) activity and cytotoxicity of **19a–b** and **20a–d** in MT-4 cells.

Compd.	$R_1$	Y	$EC_{50}$ (nmol/L) <sup>a</sup>		$CC_{50}$ ( $\mu$ mol/L) <sup>b</sup>
			IIIB	RES056	
<b>19a</b>	CN	N	>3081	ND <sup>c</sup>	19.3 ± 3.04
<b>19b</b>	CN	CHNH	>16,086	ND	3.07 ± 0.30
<b>20a</b>	CN	–	233 ± 158	>248,390	>284
<b>20b</b>	CV	–	20.0 ± 19.8	22,659 ± 4857	142 ± 31.1
<b>20c</b>	CH <sub>3</sub>	–	523 ± 466	>152,494	152 ± 28.3
<b>20d</b>	CN	–	5690 ± 4760	ND	20.5 ± 11.3
NVP	–	–	118 ± 66.9	2221 ± 736	>15.0
EFV	–	–	2.67 ± 1.73	114 ± 55.6	>6.34
ETR	–	–	2.81 ± 0.47	35.2 ± 19.7	2.20 ± 0.015
RPV	–	–	1.00 ± 0.27	10.7 ± 7.96	3.98

<sup>a</sup> $EC_{50}$ : concentration of compound required to achieve 50% protection of MT-4 cell cultures against HIV-1-induced cytopathicity, as determined by the MTT method.

<sup>b</sup> $CC_{50}$ : concentration required to reduce the viability of mock-infected cell cultures by 50%, as determined by the MTT method.

<sup>c</sup>ND: not determined.

**Table 3** Anti-HIV-1 (IIIB and RES056) activity and cytotoxicity of **23a–i** and **27a–b** in MT-4 cells.


Compd.	R <sub>1</sub>	R <sub>2</sub>	EC <sub>50</sub> (nmol/L) <sup>a</sup>		CC <sub>50</sub> (μmol/L) <sup>b</sup>
			IIIB	RES056	
<b>23a</b>	CN	4-CN	4.44 ± 1.39	263 ± 97.1	3.76 ± 0.32
<b>23b</b>	CN	3-CN	6.00 ± 1.03	764 ± 86.1	3.78 ± 0.63
<b>23c</b>	CN	2-CN	7.10 ± 2.69	1158 ± 184	3.86 ± 1.14
<b>23d</b>	CN	3-SO <sub>2</sub> NH <sub>2</sub>	4.65 ± 0.65	790 ± 134	5.61 ± 3.42
<b>23e</b>	CN	4-CO <sub>2</sub> C <sub>2</sub> H <sub>5</sub>	14.8 ± 13.5	4834 ± 517	65.3 ± 39.8
<b>23f</b>	CN	4-NH <sub>2</sub>	7.00 ± 1.04	653 ± 236	12.0 ± 6.47
<b>23g</b>	CN	4-NHSO <sub>2</sub> CH <sub>3</sub>	2.37 ± 1.98	326 ± 185	≥3.87
<b>23h</b>	CV	4-SO <sub>2</sub> NH <sub>2</sub>	3.43 ± 2.00	15.2 ± 9.44	3.31 ± 1.70
<b>23i</b>	CH <sub>3</sub>	4-SO <sub>2</sub> NH <sub>2</sub>	5.43 ± 4.40	442 ± 272	≥226
<b>27a</b>	CN	3-CN	10.2 ± 7.57	836 ± 290	8.39 ± 5.22
<b>27b</b>	CN	3-CONH <sub>2</sub>	3.76 ± 2.29	24.5 ± 8.11	5.99 ± 2.95
NVP	–	–	118 ± 66.9	2221 ± 736	>15.0
EFV	–	–	2.67 ± 1.73	114 ± 55.6	>6.34
ETR	–	–	2.81 ± 0.47	35.2 ± 19.7	2.20 ± 0.015
RPV	–	–	1.00 ± 0.27	10.7 ± 7.96	3.98

<sup>a</sup>EC<sub>50</sub>: concentration of compound required to achieve 50% protection of MT-4 cell cultures against HIV-1-induced cytopathicity, as determined by the MTT method.

<sup>b</sup>CC<sub>50</sub>: concentration required to reduce the viability of mock-infected cell cultures by 50%, as determined by the MTT method.

**23a** (4-CN) ≈ **23g** (4-NHSO<sub>2</sub>CH<sub>3</sub>) > **23f** (4-NH<sub>2</sub>) > **23e** (4-CO<sub>2</sub>C<sub>2</sub>H<sub>5</sub>), demonstrating that suitably sized substituents containing hydrogen-bond donors and acceptors are more beneficial for inhibitory activity. In agreement with the previously established SAR, the replacement of the methyl at the R<sub>1</sub> position with a cyanovinyl led to remarkably improved antiviral activities especially against the RES056 strain, as exemplified by compounds **23i** (CH<sub>3</sub>, EC<sub>50(RES056)</sub> = 442 nmol/L) and **23h** (CV, EC<sub>50(RES056)</sub> = 15.2 nmol/L). In addition, the contribution of directly linked substituted phenyl on the piperidine moiety to the inhibitory potency was also investigated. Specifically, removal of the methylene linker of compound **23b** yielded a slightly less potent compound **27a**; while replacing the cyano group of **27a** with an amide group significantly elevated the activities (**27b**, EC<sub>50(IIIB)</sub> = 3.76 nmol/L, EC<sub>50(RES056)</sub> = 24.5 nmol/L), but still inferior to those of compound **23h** (EC<sub>50(IIIB)</sub> = 3.43 nmol/L, EC<sub>50(RES056)</sub> = 15.2 nmol/L).

Based on the preliminary antiviral activities, several potent compounds were further evaluated against various NNRTI-resistant strains. As illustrated in Table 4, all compounds demonstrated excellent potency against HIV-1 variants at nanomolar levels, with EC<sub>50</sub> values ranging from 2.30 to 184 nmol/L.

In terms of the L100I strain<sup>38,39</sup>, all selected compounds were more potent than EFV (EC<sub>50</sub> = 57.4 nmol/L) with EC<sub>50</sub> values of 4.46–55.6 nmol/L, among which **23h** (EC<sub>50</sub> = 4.46 nmol/L) and **15b** (EC<sub>50</sub> = 7.26 nmol/L) showed 2.0 times and 1.3 times greater activity than ETR (EC<sub>50</sub> = 9.13 nmol/L), although inferior to RPV (EC<sub>50</sub> = 1.54 nmol/L). With respect to the K103N strain<sup>40,41</sup>, all compounds were endowed with excellent potency in the single-digit

nanomolar range (EC<sub>50</sub> = 2.30–8.69 nmol/L), being more active than EFV (EC<sub>50</sub> = 99.2 nmol/L) and comparable to ETR (EC<sub>50</sub> = 3.38 nmol/L) and RPV (EC<sub>50</sub> = 1.31 nmol/L). In the case of the Y181C strain<sup>42,43</sup>, all compounds except **15a** and **23i** were more effective than ETR, while **23h** (EC<sub>50</sub> = 8.46 nmol/L) demonstrated a 1.7-fold improvement in potency compared to ETR (EC<sub>50</sub> = 14.1 nmol/L). As regards the Y188L strain<sup>44</sup>, all of them inhibited Y188L strain more potently than RPV (EC<sub>50</sub> = 79.4 nmol/L) and EFV (EC<sub>50</sub> = 93.2 nmol/L), with EC<sub>50</sub> values below 43.0 nmol/L, and **23h** (EC<sub>50</sub> = 16.5 nmol/L) yielded equipotent activity to ETR (EC<sub>50</sub> = 15.4 nmol/L). For the E138K strain selected in a high proportion of patients receiving RPV<sup>45,46</sup>, **23g** (EC<sub>50</sub> = 8.66 nmol/L) displayed the best potency, which was slightly superior to ETR (EC<sub>50</sub> = 10.7 nmol/L) but less potent than RPV (EC<sub>50</sub> = 5.75 nmol/L). In terms of the highly resistant double-mutant strain F227L + V106A<sup>47,48</sup>, most compounds remained very potent inhibition of replication of this strain. In particular, **23h** provided optimal efficacy of 5.35 nmol/L, which was up to 15.3- and 14.5-fold better than RPV (EC<sub>50</sub> = 81.6 nmol/L) and EFV (EC<sub>50</sub> = 77.4 nmol/L), respectively.

Therefore, **23h** was identified as the most potent inhibitor against mutant strains. Fig. 5 clearly presented a visual comparison of the anti-HIV-1 potency of **23h** versus the reference drugs ETR and EFV, indicating that **23h** had higher inhibitory effects on all strains than the reference drugs, especially for the highly resistant double-mutant strains K103N + Y181C and F227L + V106A.

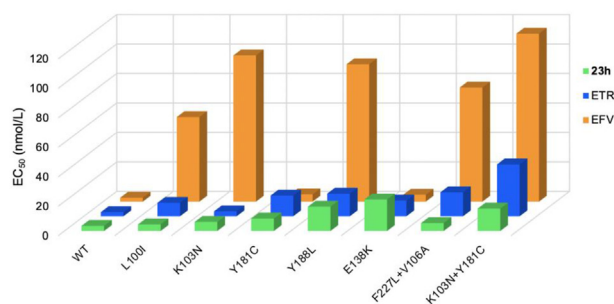
Furthermore, the SI and RF values of the selected compounds against the mutant strain are listed in Table 5. To be specific, most



**Table 4** Anti-HIV-1 activity against resistant strains of the representative target compounds.

Compd.	EC <sub>50</sub> (nmol/L) <sup>a</sup>					
	L100I	K103N	Y181C	Y188L	E138K	F227L + V106A
<b>15a</b>	16.7 ± 4.51	6.41 ± 0.99	42.3 ± 4.45	20.7 ± 1.88	17.4 ± 2.24	40.9 ± 0.00
<b>15b</b>	7.26 ± 0.51	6.42 ± 0.40	11.1 ± 3.39	23.3 ± 0.48	21.7 ± 7.55	27.9 ± 9.17
<b>16b</b>	21.8 ± 5.65	2.30 ± 0.15	10.4 ± 1.44	12.3 ± 2.27	10.9 ± 0.32	37.9 ± 21.3
<b>23f</b>	55.6 ± 2.68	8.69 ± 0.00	14.7 ± 1.17	26.1 ± 3.53	21.6 ± 0.56	184 ± 8.33
<b>23g</b>	28.0 ± 5.38	4.59 ± 0.45	≤8.29	12.7 ± 2.99	8.66 ± 0.54	165 ± 40.8
<b>23h</b>	4.46 ± 0.36	6.13 ± 0.12	8.46 ± 1.17	16.5 ± 5.18	21.4 ± 4.19	5.35 ± 0.69
<b>23i</b>	39.2 ± 7.66	6.56 ± 1.07	35.7 ± 5.75	43.0 ± 0.26	37.6 ± 7.41	64.7 ± 13.3
<b>27b</b>	13.3 ± 6.79	5.46 ± 0.00	7.87 ± 1.84	7.14 ± 1.50	17.1 ± 4.42	111 ± 11.4
NVP	705 ± 451	3551 ± 2413	3785 ± 2577	4416 ± 2469	158 ± 112	3538 ± 2750
EFV	57.4 ± 45.9	99.2 ± 56.8	4.94 ± 1.75	93.2 ± 58.9	4.67 ± 1.38	77.4 ± 55.9
ETR	9.13 ± 6.10	3.38 ± 0.69	14.1 ± 5.72	15.4 ± 6.07	10.7 ± 6.66	16.3 ± 6.24
RPV	1.54 ± 0.00	1.31 ± 0.36	4.73 ± 0.48	79.4 ± 0.77	5.75 ± 0.11	81.6 ± 21.2

<sup>a</sup>EC<sub>50</sub>: concentration of compound required to achieve 50% protection of MT-4 cell cultures against HIV-1-induced cytopathicity, as determined by the MTT method.

**Figure 5** Comparison of the *in vitro* antiviral activity of **23h**, ETR, and EFV.

compounds had relatively higher SI values of 155–34,451 than ETR (SI = 63–651) and RPV (SI = 49–3045) toward the mutant strains due to their decreased cytotoxicity. Intriguingly, all compounds showed no obvious decline in activity against the K103N strain compared to that against the WT strain, as reflected by an RF value of less than 2.0 (RF = 1.2–2.0). In addition, the RF values of **23h** (RF = 1.6 and 4.4) were lower than those of ETR (RF = 5.8

and 12.5), EFV (RF = 29.0 and 42.7), and RPV (RF = 82 and 10.7) for the challenging variants F227L + V106A and K103N + Y181C. More importantly, **23h** had a major improvement in drug resistance profiles (RF = 1.3–6.2) compared to ETR (RF = 1.2–12.5), EFV (RF = 1.7–42.7), and RPV (RF = 1.3–82), suggesting that **23h** featuring the flexible scaffold is more resilient to clinically relevant NNRTI-resistant mutations.

On the whole, the above biological evaluation results and comprehensive SAR investigations reasonably verified our original design hypotheses: i) the non-planar dihydrothiopyran ring introduced into the central scaffold could accommodate well in the tolerant region II to develop extensive interactions; ii) the cyanovinyl group is the optimal substituent on the left-wing because of the formation of additional  $\pi$ – $\pi$  stacking interactions; iii) the benzyl-linked aminopiperidine moiety on the right wing proved to be more favorable for improving activity, due to the flexible conformation enables relatively easy adaptation to the residue mutations; and these systematic optimization campaigns led to the identification of the most promising inhibitor **23h** with robust antiviral potency and improved resistance profiles against NNRTI-resistant strains.

**Table 5** Selectivity index and resistance fold for HIV-1 variants of the representative target compounds.

Compd.	SI <sup>a</sup> (RF <sup>b</sup> )						
	L100I	K103N	Y181C	Y188L	E138K	F227L + V106A	RES056
<b>15a</b>	271 (4.9)	707 (1.9)	107 (12.5)	219 (6.1)	260 (5.1)	111 (12.1)	53 (25.2)
<b>15b</b>	674 (2.3)	762 (2.0)	441 (3.5)	210 (7.3)	225 (6.8)	175 (8.8)	208 (7.4)
<b>16b</b>	858 (15.1)	8130 (1.6)	1798 (7.2)	1520 (8.5)	1716 (7.6)	493 (26.3)	381 (34.1)
<b>23f</b>	216 (7.9)	1381 (1.2)	816 (2.1)	460 (3.7)	556 (3.0)	65 (26.3)	18 (93.3)
<b>23g</b>	≥138 (11.8)	≥843 (1.9)	≥467 (≤3.5)	≥305 (5.4)	≥447 (3.7)	≥23 (69.6)	≥12 (138)
<b>23h</b>	742 (1.3)	540 (1.8)	391 (2.5)	201 (4.8)	155 (6.2)	619 (1.6)	218 (4.4)
<b>23i</b>	≥5765 (7.2)	≥34,451 (1.2)	≥6331 (6.6)	≥5256 (7.9)	≥6011 (6.9)	≥3493 (11.9)	≥511 (81.4)
<b>27b</b>	450 (3.5)	1097 (1.5)	761 (2.1)	839 (1.9)	350 (4.5)	54 (29.5)	244 (6.5)
NVP	>21 (6.0)	>4 (30.0)	>4 (32.0)	>3 (37.4)	>95 (1.3)	>4 (30.0)	>7 (18.8)
EFV	>110 (21.5)	>64 (37.2)	>1283 (1.9)	>68 (34.9)	>1358 (1.7)	>82 (29.0)	>56 (42.7)
ETR	241 (3.2)	651 (1.2)	156 (5.0)	143 (5.5)	206 (3.8)	135 (5.8)	63 (12.5)
RPV	2575 (1.5)	3045 (1.3)	841 (4.7)	50 (80)	692 (5.8)	49 (82)	371 (10.7)

<sup>a</sup>SI: selectivity index, the ratio of CC<sub>50</sub>/EC<sub>50</sub>.

<sup>b</sup>RF: resistance fold, the ratio of EC<sub>50</sub> (mutant strain)/EC<sub>50</sub>(WT strain).

### 2.3. HIV-1 RT inhibition assay

To further validate the target of the novel dihydrothiopyrano[3,2-*d*]pyrimidine derivatives, the representative compounds **15b** and **16b** featuring *p*-cyanoaniline and **23h** featuring piperidine-linked benzyl sulfonamide were tested for their potency in inhibiting the RT enzyme. As shown in Table 6, all tested compounds

**Table 6** HIV-1 RT inhibitory activity of **15b**, **16b**, **23h**, NVP, EFV, ETR, and RPV.

Compd.	IC <sub>50</sub> (μmol/L) <sup>a</sup>	Compd.	IC <sub>50</sub> (μmol/L) <sup>a</sup>
<b>15b</b>	0.101 ± 0.012	EFV	0.014 ± 0.002
<b>16b</b>	0.027 ± 0.011	ETR	0.232 ± 0.036
<b>23h</b>	0.529 ± 0.142	RPV	0.118 ± 0.027
NVP	0.089 ± 0.015		

<sup>a</sup>IC<sub>50</sub>: inhibitory concentration of test compounds required to inhibit biotin deoxyuridine triphosphate (biotin-dUTP) incorporation into HIV-1 RT by 50%.

demonstrated potent inhibition of RT with IC<sub>50</sub> values ranging from 0.027 to 0.529 μmol/L, which were superior or comparable to that of ETR (IC<sub>50</sub> = 0.232 μmol/L) and RPV (IC<sub>50</sub> = 0.118 μmol/L). In general, the enzymatic assay results were able to suggest that these novel dihydrothiopyrano[3,2-*d*]pyrimidines showed high binding affinity to RT and belonged to typical HIV-1 NNRTIs.

### 2.4. Molecular docking analysis

To achieve insight into the theoretical binding modes of novel compounds within RT and elucidate the unique resistance profiles of **23h**, molecular docking analysis of **23h** and ETR were performed by SYBYL-X 2.0. Four co-crystal structures of WT RT (PDB ID: 6C0N)<sup>49</sup>, L100I RT (PDB ID: 1S1V)<sup>50</sup>, F227L + V106A RT (PDB ID: 6DUF)<sup>49</sup>, and K103N + Y181C RT (PDB ID: 6C0R)<sup>49</sup> were chosen as the templates.

As expected, **23h** binds to WT, L100I, F227L + V106A, and K103N + Y181C RT in a similar manner. As displayed in Fig. 6, compound **23h** adopts a typical U-shaped conformation that

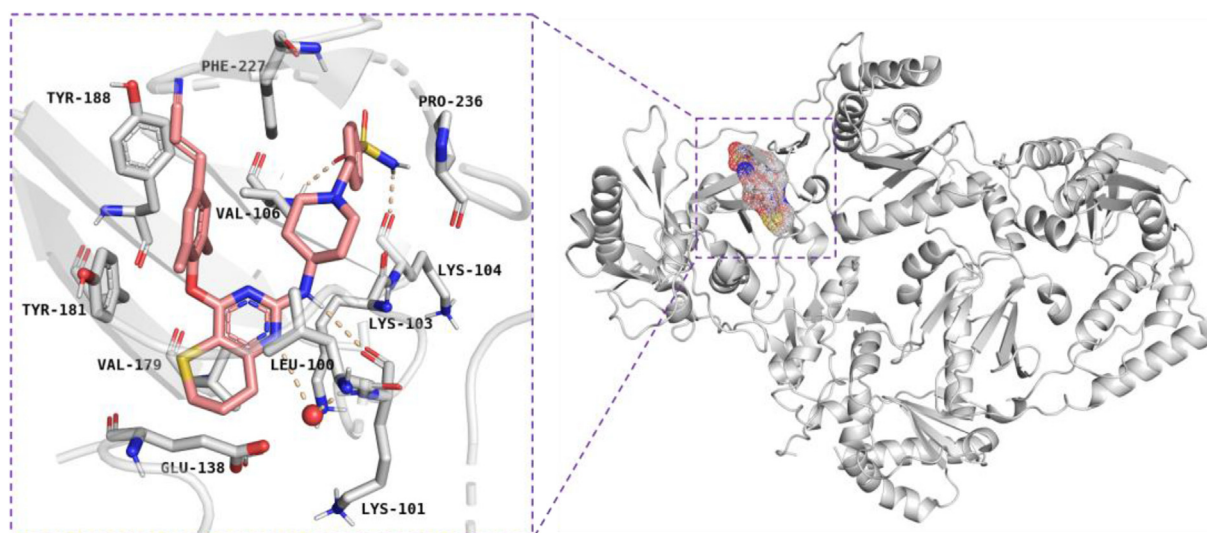


**Figure 6** Binding modes and interaction forces of **23h** (pink) with WT RT (PDB code: 6C0N).

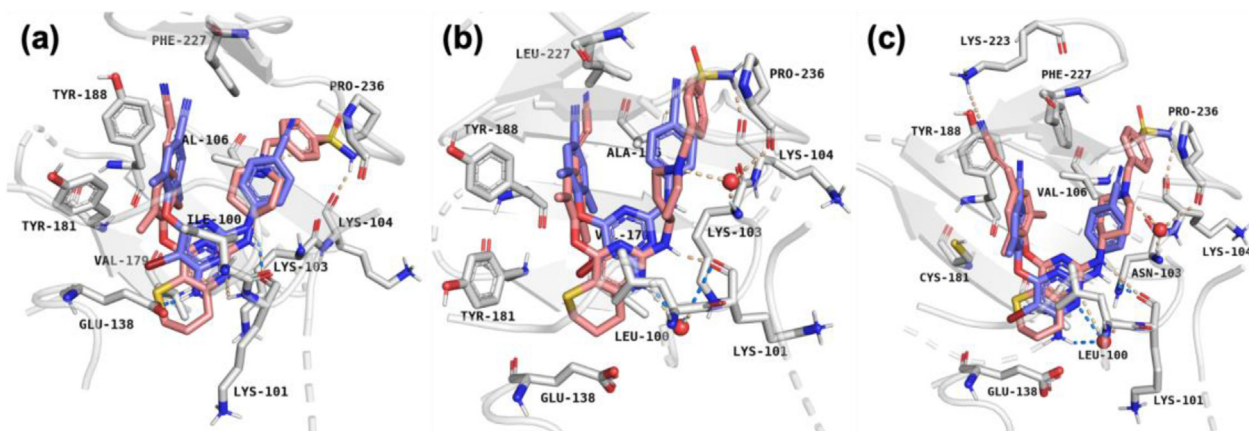


**Figure 7** (a) Superimposition of **23h** (pink) and ETR (blue) with L100I RT (PDB code: 1S1V). (b) Superimposition of **23h** (pink) and ETR (blue) with F227L + V106A RT (PDB code: 6DUF). (c) Superimposition of **23h** (pink) and ETR (blue) with K103N + Y181C RT (PDB code: 6C0R).

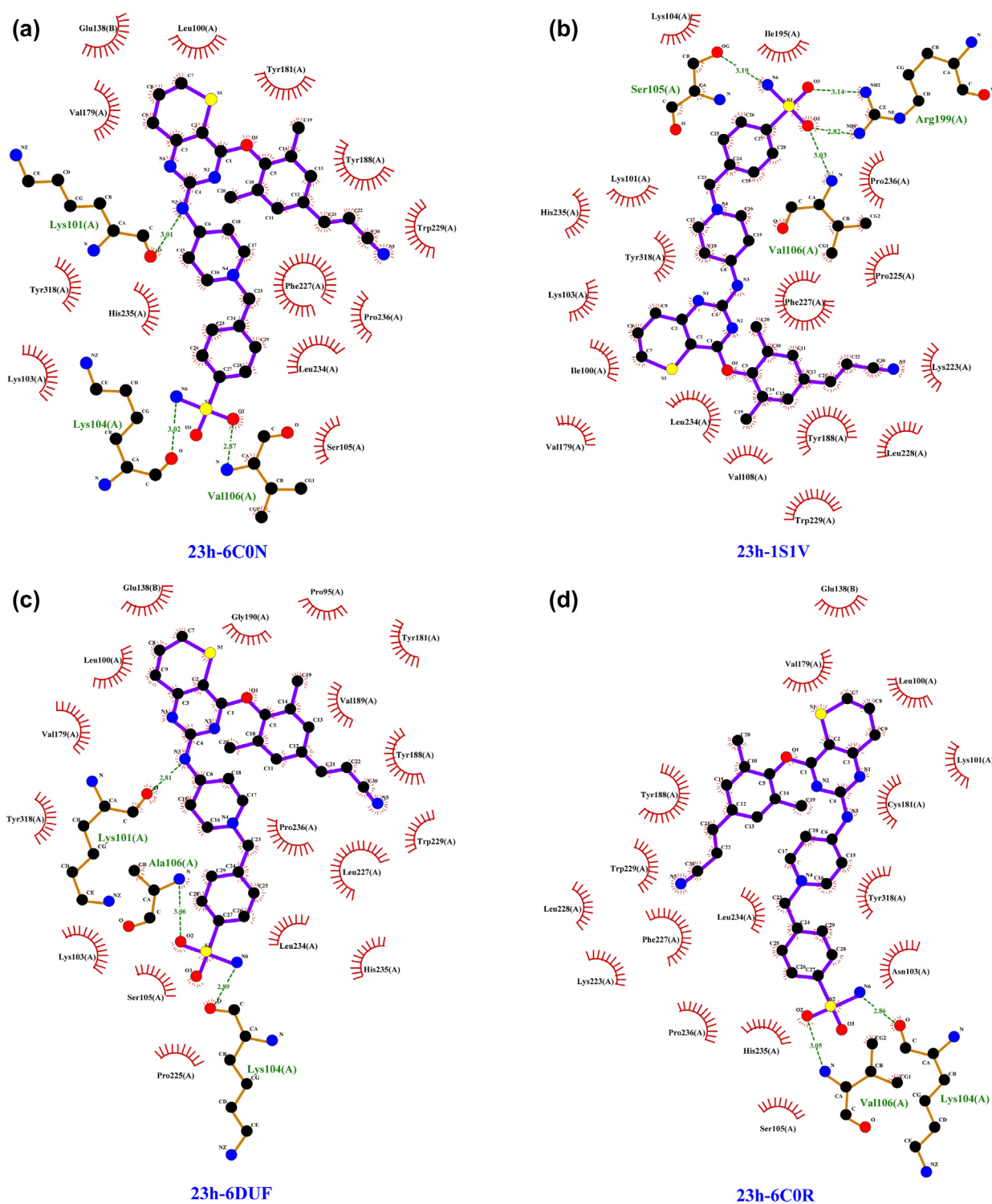


**Figure 8** Binding modes in the most abundant clusters of **23h** in complex with WT RT (a, PDB code: 6C0N), L100I RT (b, PDB code: 1S1V), F227L + V106A RT (c, PDB code: 6DUF), and K103N + Y181C RT (d, PDB code: 6C0R).

resembles other DAPY-typed inhibitors. Several common binding features and protein–ligand interactions were delineated as follows. Firstly, the left-wing of 4-cyanovinyl-2,6-dimethylphenyl moiety as a conjugated system effectively occupies the hydrophobic channel, establishing foremost  $\pi$ –stacking interactions with Tyr181 and Tyr188. Secondly, the central dihydrothiopyrano

ring is oriented towards the solvent-exposed tolerant region II, which is stabilized by non-polar interaction with Glu138 and electrostatic interaction with Leu100 and Val179. Thirdly, the pyrimidinyl and the NH linker form the “signature” dual hydrogen-bonds with the amino hydrogen ( $N\cdots H_2-O\cdots H-N$ ) and carbonyl oxygen ( $N-H\cdots O=C$ ) of the main chain of Lys101,

respectively, which are necessary to maintain binding affinity. Fourthly, the benzyl sulfonamide motif stretches into the solvent-exposed tolerant region I, being involved in double hydrogen-bonding interactions with Lys104 ( $N-H_2 \cdots O=C$ ) and Val106 ( $S=O_2 \cdots H-N$ ).

On the other hand, compound **23h** and the lead compound ETR were docked into the mutant RT simultaneously to explain the improved anti-resistance profiles of **23h**. Examination of the interaction forces between **23h** and L100I RT (Fig. 7a) indicates that the pivotal hydrogen bonds are still retained, despite slight variations in the bond distance and formation condition of the hydrogen bonds. However, one of the key hydrogen bonds between ETR and Lys101 is lost because the disappearance of electrostatic interaction caused by the L100I mutation shifted the pyrimidine ring of ETR away from the main chain of Lys101. As shown in Fig. 7b, the smaller Leu227 and Ala106 further broaden the chemical space of the pocket, allowing **23h** to occupy the binding sites through the conformational reorientation of the piperidine ring and the dihydrothiopyrano ring. Furthermore, it is observed that the “water bridge” hydrogen bonds between the piperidine ring and Lys103 ( $N \cdots H_2-O \cdots H-N$ ) and Pro236 ( $N \cdots H-O-H \cdots O=C$ ) and the hydrogen bond between sulfonamide and new Ala106 ( $S=O_2 \cdots H-N$ ) compensated for the lack of hydrophobic interaction with the highly conserved residue Phe227. By contrast, ETR can only develop one hydrogen bond with Lys101 ( $N-H_2 \cdots O-H_2 \cdots O=C$ ) through the amino group on the central ring in the presence of a bridging water molecule, whereas the double hydrogen bonds of the pyrimidine nitrogen and the NH linker with Lys101 disappears. With regard to the binding modes in K103N + Y181C RT (Fig. 7c), the nitrogen atom on the pyrimidine ring of ETR generates an intramolecular

hydrogen bond ( $N \cdots H_2-O \cdots H_2-N$ ) with its amino group instead of Lys101 *via* a water molecule, while it has no substantial contribution to the binding affinity. Of particular note are the water bridge hydrogen bonds formed with mutant Asn103 ( $N \cdots H_2-O \cdots H-N$ ) and Pro236 ( $N \cdots H-O-H \cdots O=C$ ) and the dual hydrogen bonds formed with Lys101 ( $N \cdots H_2-O \cdots H-N$ ;  $N-H \cdots O=C$ ) of **23h** continue to be maintained to offset the damage of the K103N mutation. Besides, the left-wing terminal cyano group of **23h** develops an additional hydrogen bond with the amino group of Lys223 ( $C \equiv N \cdots H_2-N$ ), compensating for the affinity loss of the weakened  $\pi-\pi$  stacking interaction caused by the Y181C substitution.

All in all, the molecular docking results clearly revealed the binding modes and interaction forces of **23h** and rationalized its potent inhibitory activity against mutant strains compared to ETR, which provides valuable information for further drug design.

## 2.5. Molecular dynamics simulation

To study the stability state and dynamic behaviors of compound **23h** binding to distinct RT, comprehensive molecular dynamics (MD) simulations of **23h** in complex with WT RT and various mutant RTs were performed for 200 ns using the software Schrödinger. All the results were visualized by the softwares LigPlot<sup>+</sup> v.2.2.8 and Schrödinger and the methods were described in the experimental section.

The MD simulation trajectories were clustered using the trajectory clustering program and the most abundant clusters of RT/**23h** complexes were extracted shown in Fig. 8, still maintaining the horseshoe conformation and interaction profile similar to those in Figs. 6 and 7. The Root Mean Square

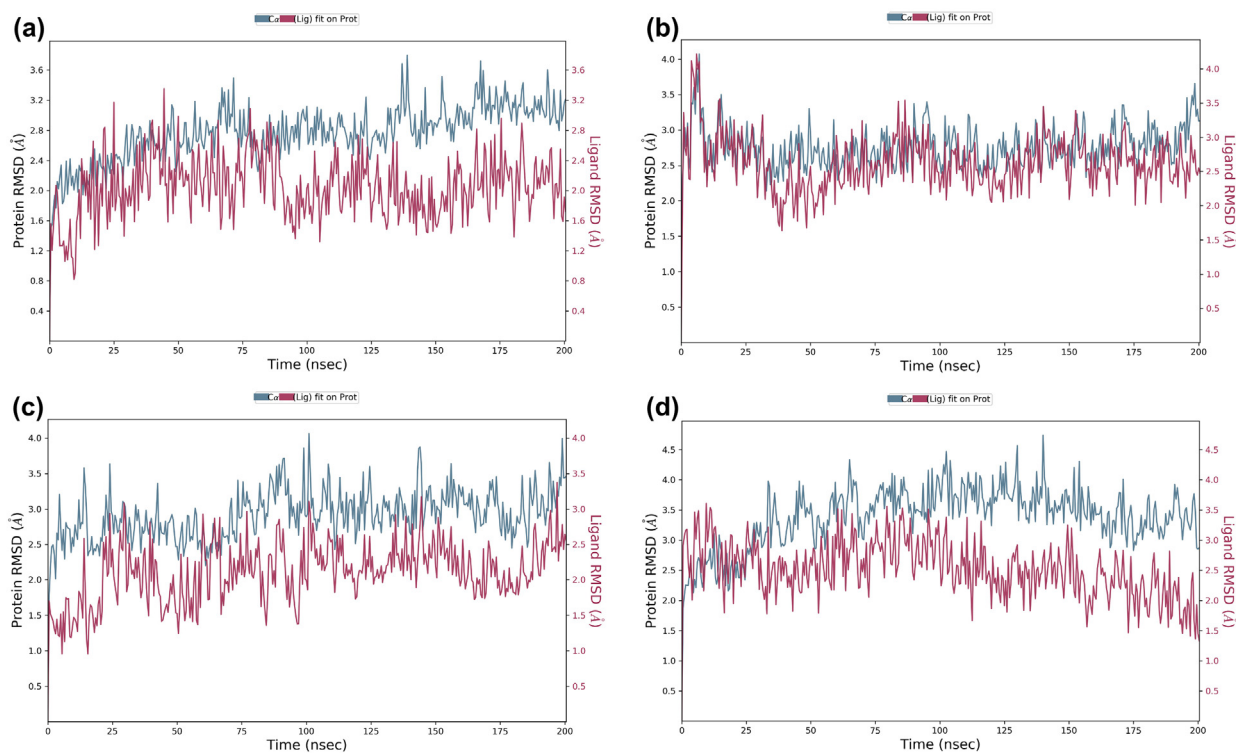


**Figure 9** RMSD–time profiles of protein-ligand complexes with reference to the first frame for the **23h**/WT RT complex (a), **23h**/L100I RT complex (b), **23h**/F227L + V106A RT complex (c), and **23h**/K103N + Y181C RT complex (d) during the 200 ns MD simulations.

Deviation (RMSD) values are commonly used to assess the conformational drift of protein-ligand complexes by measuring the average shift change of atoms in a specific frame relative to the reference frame. As depicted in Fig. 9, the RMSD plots indicated that all the HIV-1 RT-ligand complexes remain stable during the 200 ns simulation process, indicating that the overall structure of the RT proteins did not change significantly due to the binding of the **23h** ligand. In addition, the coordinates of **23h** fluctuate less than 2.5 Å in each RT/**23h** complex after 200 ns of MD simulations and consistently bind stably to the HIV-1 RT allosteric site. The Root Mean Square Fluctuation (RMSF) of RT and **23h** were further investigated to characterize the local deviation of protein chain and ligand atom positions, respectively. The peaks on the protein RMSF plot indicate the amino acid residues that fluctuate the most during the simulation (Supporting Information Fig. S1), while the ligand RMSF plot shows the ligand fluctuations for each atom of the **23h** backbone, corresponding to the two-dimensional structure in the top

panel (Supporting Information Fig. S2). In addition, Ramachandran plots showed that all RT residues were located in the most favoured (more than 90%), additional allowed, and generously allowed regions (Fig. 10).

Protein-ligand contacts of **23h** with different RTs are illustrated in Figs. 11 and 12, and Supporting Information Fig. S3, which demonstrate the detailed interactions between the ligand and specific residues, mainly including hydrogen bond, hydrophobic contact, and water bridge. Notably, the interactions fraction plot implies that the specific interaction remains constant over what percent of the 200 ns simulations, while multiple contacts between individual residues and the ligand may yield interaction fraction above 1.0 (Fig. 11). Besides, Fig. 12 visually represents the number of contact forces between **23h** and RT in each trajectory frame, as well as the specific residue codes that interact with the ligand, with darker orange reflecting stronger interactions. Consistent with the results in Figs. 11 and 12, the two-dimensional ligand interaction diagrams demonstrated that **23h**

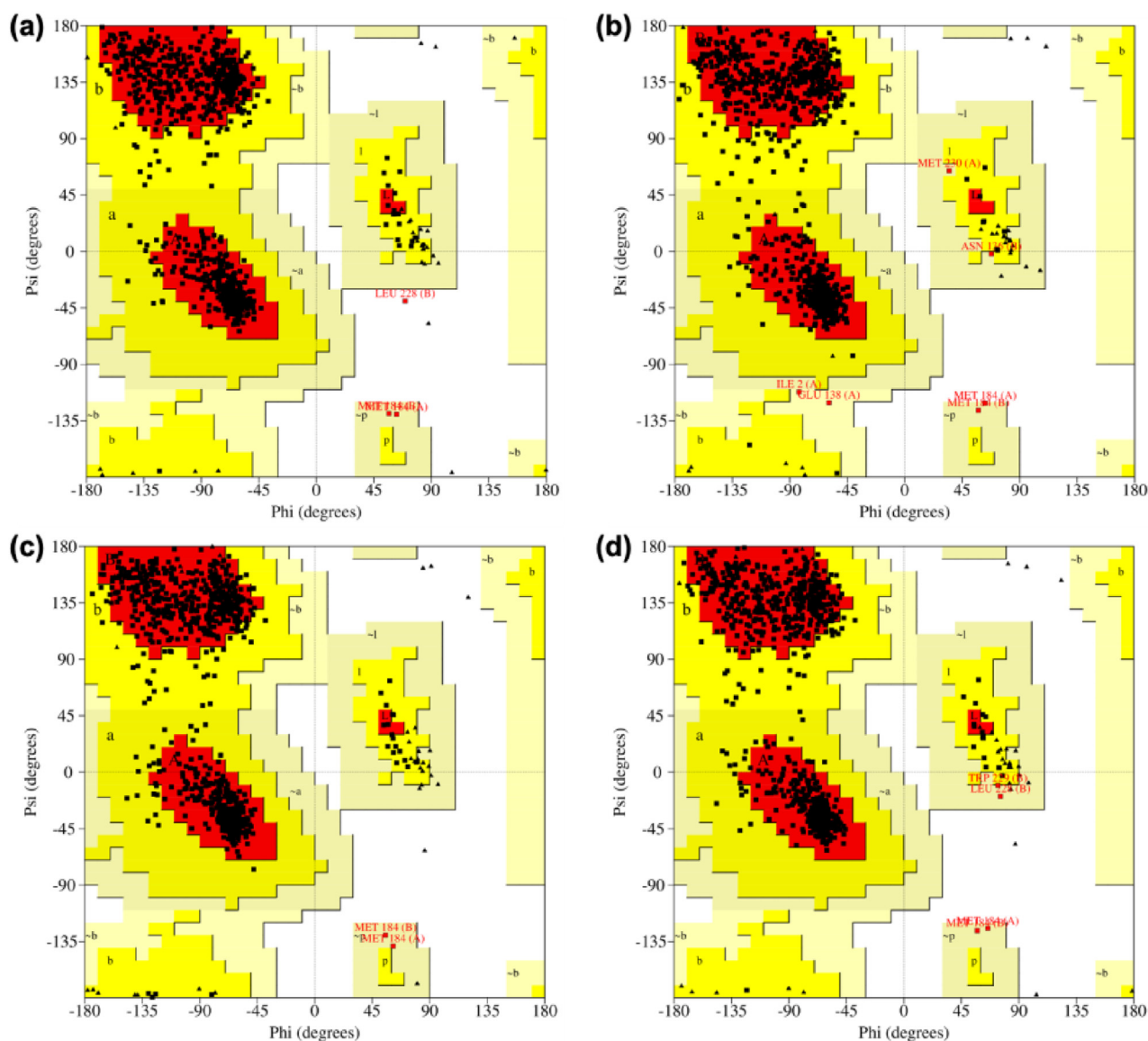


**Figure 10** Ramachandran plots of the **23h**/WT RT complex (a), **23h**/L100I RT complex (b), **23h**/F227L + V106A RT complex (c), and **23h**/K103N + Y181C RT complex (d) after 200 ns MD simulations.



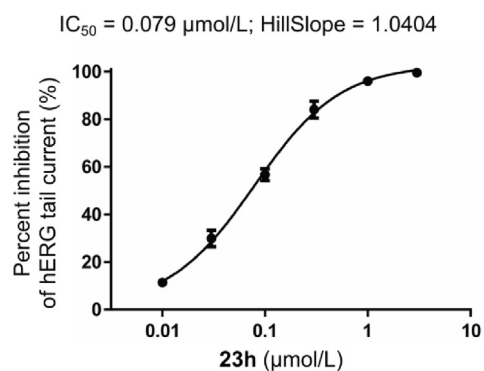


**Figure 13** Inhibitory activity of compound **23h** against the hERG channel.

**Table 8** Water solubility of compound **23h**, ETR, and RPV.

Compd.	<b>23h</b>	ETR	RPV
pH = 7.4 ( $\mu\text{g/mL}$ )	3.04	<1	<1
pH = 7.0 ( $\mu\text{g/mL}$ )	11.7	<1	0.02
pH = 2.0 ( $\mu\text{g/mL}$ )	161	127	103

establishes signature double hydrogen bonds with the Lys101 backbone of both WT RT and mutant RT and forms extensive hydrophobic contacts with Tyr181, Tyr188, and Trp229,

contributing to the critical role of maintaining the protein-ligand binding affinity (Fig. S3).

Overall, the MD simulation results indicated that the complexes of ligand **23h** with both WT RT and mutant RT maintained stable conformations and retained extensive protein-ligand interactions, and Ramachandran plots validated the structural stability of all RT/**23h** complex, contributing to the high binding affinity between **23h** and various RTs.

## 2.6. CYP450 inhibitory activity assessment

Four main subtypes of cytochrome P450 (CYP) enzymes, CYP2C9, CYP2C19, CYP2D6, and CYP3A4, are widely involved in the metabolism of most drugs *in vivo* and play a crucial role in detoxification and bioactivation processes<sup>51</sup>. ETR and RPV have potent CYP inhibitory activity for CYP2C9 and CYP2C19, thus may cause adverse drug–drug interactions in combination with other antiviral agents<sup>52,53</sup>. Therefore, compound **23h** was further evaluated for its CYP enzymatic inhibitory activity to predict the risk of combination administration, with selective enzyme inhibitors as positive controls. As displayed in Table 7, **23h** showed no or weak CYP450 inhibitory potency against CYP1A2 ( $IC_{50} > 50 \mu\text{mol/L}$ ), CYP2C9 ( $IC_{50} = 3.41 \mu\text{mol/L}$ ), CYP2C19 ( $IC_{50} = 15.6 \mu\text{mol/L}$ ), and CYP2D6 ( $IC_{50} = 36.8 \mu\text{mol/L}$ ), which were much lower than those of ETR ( $IC_{50} = 0.277\text{--}12.0 \mu\text{mol/L}$ ) and RPV ( $IC_{50} = 0.335\text{--}9.11 \mu\text{mol/L}$ ). In particular, the inhibitory effects of **23h** on CYP2C9 and CYP2C19 were significantly reduced compared to ETR and RPV.

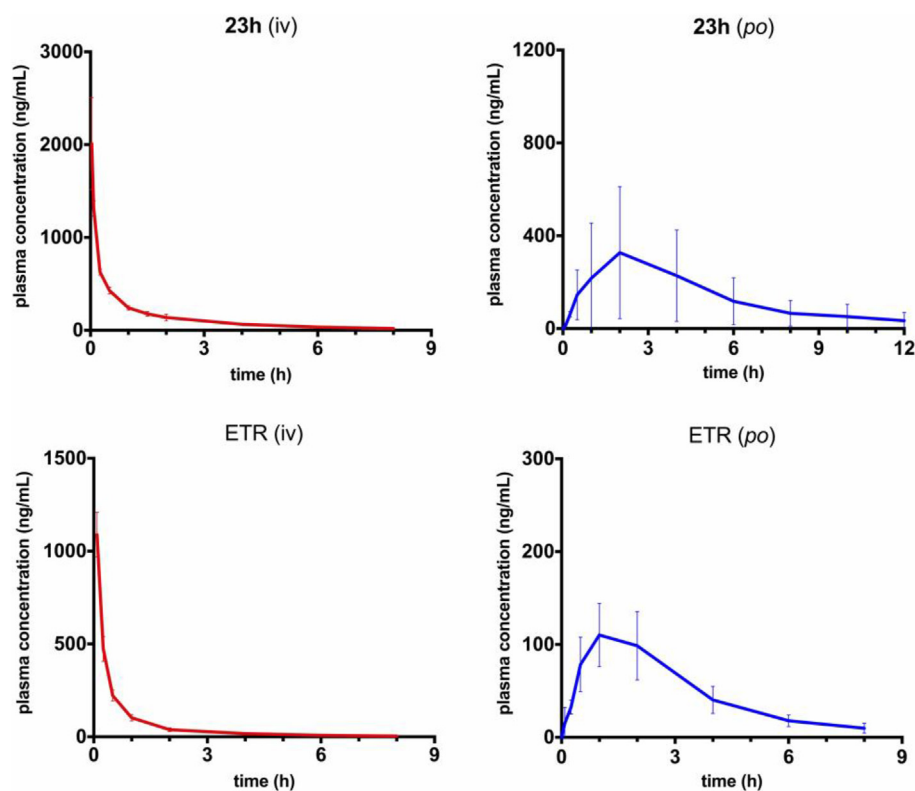


**Figure 14** Drug–time curve of **23h** and ETR after iv and *po* administration.

**Table 9** Pharmacokinetic profiles of compound **23h** and ETR.

Parameter <sup>a</sup>	Unit	<b>23h</b> (iv) <sup>b</sup>	<b>23h</b> (po) <sup>c</sup>	ETR (iv) <sup>b</sup>	ETR (po) <sup>c</sup>
$t_{1/2}$	h	2.09 ± 0.39	3.00 ± 0.74	1.80 ± 0.24	1.82 ± 0.07
$T_{max}$	h	—	1.50 ± 0.87	—	1.00 ± 0.00
$C_{max}$	µg/L	—	333 ± 276	—	110 ± 34.1
$AUC_{0-t}$	µg/L·h	1152 ± 69.7	1685 ± 1480	576 ± 45	395 ± 139
$AUC_{0-\infty}$	µg/L·h	1211 ± 78.9	1857 ± 1678	587 ± 48	421 ± 153
$V$	L/kg	49.7 ± 9.00	—	8.85 ± 1.17	—
CL	L/h/kg	16.6 ± 1.07	—	3.42 ± 0.30	—
$MRT_{0-t}$	h	1.56 ± 0.17	4.10 ± 0.12	0.93 ± 0.23	2.55 ± 0.04
$MRT_{0-\infty}$	h	2.03 ± 0.41	5.02 ± 0.48	1.10 ± 0.34	3.03 ± 0.14
$F$	%	15.33	—	7.17	—

<sup>a</sup>PK parameter (mean ± SD,  $n = 3$ ).

<sup>b</sup>Dosed intravenously at 2 mg/kg.

<sup>c</sup>Dosed orally at 20 mg/kg.

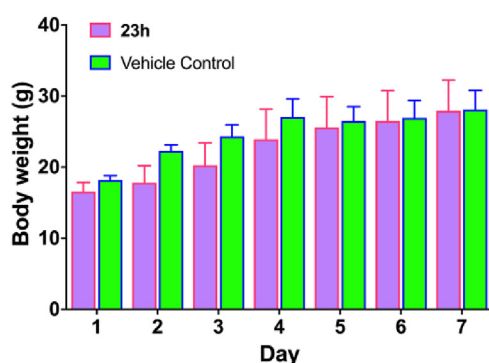


**Figure 15** The single-dose acute toxicity of **23h** after oral administration.

Overall, compound **23h** showed no apparent inhibition of the major CYP isoforms, with improved CYP inhibition profiles over ETR and RPV.

### 2.7. hERG channel inhibition assay

The human ether-à-go-go-related gene (hERG) channel is responsible for the rapid repolarization of the cardiac action potential and plays a crucial role in maintaining normal cardiac function<sup>54</sup>. Blockade of the hERG channel by non-cardiovascular drugs could induce acquired long QT syndrome and increase the risk of Torsade de Pointes. In the Phase IIb clinical trial NCT00110305 of RPV, dose-dependent prolongation of the QT interval with a delayed onset was observed in healthy subjects receiving daily doses of 75 mg<sup>55</sup>. Therefore, we further determined the inhibitory activity of compound **23h** on the hERG potassium channel to assess the potential cardiac safety risk by using the manual patch-clamp electrophysiology method. As shown in Fig. 13, compound **23h** demonstrated an  $IC_{50}$  value of 0.079 µmol/L against the hERG channel, which was weaker than that of the reference drug cisapride ( $IC_{50} = 0.012$  µmol/L).

### 2.8. In vivo pharmacokinetics studies

Oral administration remains the most ideal and convenient delivery method for cART<sup>12</sup>. As shown in Table 8, compound **23h**

exhibited improved water solubility (sol. = 161 µg/mL, pH = 2.0; sol. = 11.7 µg/mL, pH = 7.0; sol. = 3.04 µg/mL, pH = 7.4), which were higher than those of ETR and RPV at different pH conditions. Therefore, the *in vivo* pharmacokinetic profiles of the most promising compound **23h** and ETR were investigated after iv and po administration (Fig. 14). After iv dose at 2 mg/kg, **23h** was characterized by a moderate half-life of 2.09 h, a favorable volume of distribution ( $V = 49.7$  L/kg), and a slow mean clearance rate ( $CL = 16.6$  L/h/kg). After po dose at 20 mg/kg, **23h** achieved the maximum plasma concentration ( $C_{max} = 333$  µg/L) at 1.50 h, and its area under curve ( $AUC_{0-\infty}$ ) and mean residence time ( $MRT_{0-\infty}$ ) was 1857 µg/L·h and 5.02 h, respectively. Especially, compound **23h** ( $t_{1/2(iv)} = 2.09$  h;  $t_{1/2(po)} = 3.00$  h) exhibited a longer half-life than ETR ( $t_{1/2(iv)} = 1.80$  h;  $t_{1/2(po)} = 1.82$  h) after iv and po administration, respectively. Moreover, **23h** displayed a favorable oral bioavailability ( $F$ ) of 15.33%, which was higher than that of ETR ( $F = 7.17\%$ ) and was sufficient for an orally bioavailable candidate (Table 9).

### 2.9. In vivo safety studies

A suitable drug candidate requires not only excellent antiviral activity and PK profiles, but also favorable *in vivo* safety properties. Therefore, the single-dose acute toxicity of **23h** was investigated to assess its *in vivo* safety properties. After intragastric administration of **23h** at 2000 mg/kg, no death or signs of intoxication were observed in the drug administration mice. Besides, there were no significant body weight loss or abnormal behaviors such as fatigue, cramps, anorexia, and ruffled fur in the treatment group compared with the control group (0 mg/kg). Body weight of treatment and control groups gradually increased in the following 7 days, with no obvious difference in weight gain (Fig. 15). Overall, the *in vivo* safety studies indicated that **23h** was well tolerated at doses up to 2000 mg/kg without acute toxicity.

## 3. Conclusions

Based on the NNRTI “four-point pharmacophore” model, we have designed and synthesized novel series of dihydrothiopyrano[3,2-*d*] pyrimidines, to fully exploit the potential chemical space and discover potent HIV-1 inhibitors with higher drug-resistance profiles and favorable pharmacological properties. Detailed SAR



investigations were derived from the biological evaluation results: (1) the saturated dihydrothiopyran ring introduced into the central scaffold could accommodate well in the tolerant region II to form extensive interactions; (2) the cyanovinyl group is the optimal substituent on the left-wing due to the prolonged conjugation system enhancing the  $\pi$ -stacking interactions; (3) the piperidine-linked benzyl moiety is more favorable for antiviral potency, suggesting that conformational flexibility allows the ligand to adapt for resistant RT mutations; (4) the dual hydrogen bonds formed by the pyrimidinyl nitrogen and the imino linker with Lys101 are essential to maintain binding affinity.

Among these newly developed derivatives, compound **23h** was identified as an exceptionally potent inhibitor against WT and resistant HIV-1 strains, with  $EC_{50}$  values of 3.43 nmol/L (IIB), 4.46 nmol/L (L100I), 6.13 nmol/L (K103N), 8.46 nmol/L (Y181C), 16.5 nmol/L (Y188L), 21.4 nmol/L (E138K), 5.35 nmol/L (F227L + V106A), and 15.2 nmol/L (K103N + Y181C). In the case of the highly resistant double-mutants K103N + Y181C and F227L + V106A, **23h** still displayed prominent inhibitory potency of 15.2 and 5.35 nmol/L, being equivalent to RPV ( $EC_{50}$  = 10.7 and 81.6 nmol/L), and more effective than EFV ( $EC_{50}$  = 114 and 77.4 nmol/L) and ETR ( $EC_{50}$  = 35.2 and 16.3 nmol/L). More encouragingly, **23h** afforded significant improvement in drug resistance profiles (RF = 1.3–6.2) against various mutant strains compared to EFV (RF = 1.7–42.7), ETR (RF = 1.2–12.5), and RPV (RF = 1.3–82). In the target validation experiment, **23h** potently inhibited HIV-1 RT at a low micromolar concentration and thus behaved as a typical NNRTI. Comprehensive molecular docking analysis and MD simulations demonstrated that the molecular mechanism of action of **23h** contributes to the elevated binding affinity, providing a reasonable explanation for the improved drug resistance profiles and guiding further structural optimization efforts. In addition, the CYP450 inhibition profiles of **23h** were significantly improved over ETR and RPV, with  $IC_{50}$  values in the range of 3.41–50  $\mu$ mol/L against the main CYP enzymes. Notably, **23h** exhibited desirable *in vivo* pharmacokinetic properties, with a higher oral bioavailability of 15.33% and a longer half-life of 3.00 h compared to ETR ( $F$  = 7.17%;  $t_{1/2}$  = 1.82 h). Furthermore, the *in vivo* safety studies indicated that **23h** showed good tolerability at the dose of 2000 mg/kg.

Taken together, the current study validated the design hypothesis of introducing alicyclic rings and hydrophilic groups into the solvent-exposed region to balance the bioactivity and physicochemical properties. Particularly, all *in vitro* and *in vivo* data highlight the potential of **23h** as an anti-HIV-1 candidate due to its prominent antiviral activities and favorable drug-ability profiles.

## 4. Experimental

### 4.1. Chemistry

Melting point (mp) was determined on the micromelting point apparatus (RY-1G, Tianjin Skylight).  $^1H$  NMR and  $^{13}C$  NMR spectra were recorded on the nuclear magnetic resonance spectrometer (Bruker Avance 400 or 600 MHz NMR Spectrometer, Bruker) with DMSO- $d_6$  or  $CDCl_3$  as the solvent and tetramethylsilane (TMS) as the internal standard. Mass spectra were obtained on the layer chromatography–mass spectrometry

(LC–MS) instrument (TSQ Vantage LC–MS/MS, Thermo Fisher). Thin-layer chromatography (TLC) was conducted on the high-efficiency thin-layer chromatography silica gel plate (Silica Gel 60 GF254, Merck) to monitor the reaction. Silica gel column chromatography was performed on the column packed with 200–300 mesh silica gel. Rotary evaporators (EYELA N-1300D, Tokyo Rikakikai) were used to concentrate the excess solvent. Sample purity was measured on a Shimadzu SPD-20A/20AV HPLC system. All compounds are >95% pure by HPLC analysis.

#### 4.1.1. Synthesis of methyl 4-((2-methoxy-2-oxoethyl)thio)butanoate (**9**)

To a solution of sodium methoxide (0.15 g, 3.0 mmol) in MeOH (10 mL) was added methyl 2-mercaptoacetate (**8**, 0.11 g, 1.0 mmol), and the mixture was stirred at room temperature for 30 min. Potassium iodide (1.66 mg, 0.01 mmol) and methyl 4-chlorobutanoate (0.14 g, 1.0 mmol) were added and the solution was stirred at 70 °C for 10 h. After cooling to room temperature, the reaction mixture was filtered and the resultant filtrate was concentrated under vacuum to remove the solvent. Then 10 mL of water was added and the mixture was extracted with EtOAc (3  $\times$  10 mL). The combined organic layer was washed with saturated brine (3  $\times$  5 mL), dried over anhydrous  $Na_2SO_4$ , filtered, and concentrated in vacuum to give intermediate **9** as a yellow oil. Yield: 83%.  $^1H$  NMR (600 MHz,  $CDCl_3$ ):  $\delta$  3.75 (s, 3H,  $SCH_2COOCH_3$ ), 3.66 (s, 3H,  $SCH_2CH_2CH_2COOCH_3$ ), 3.21 (s, 2H,  $SCH_2COOCH_3$ ), 2.77 (t,  $J$  = 7.2 Hz, 2H,  $SCH_2CH_2CH_2COOCH_3$ ), 2.66 (t,  $J$  = 7.2 Hz, 2H,  $SCH_2CH_2CH_2COOCH_3$ ), 1.93 (p,  $J$  = 7.2 Hz, 2H,  $SCH_2CH_2CH_2COOCH_3$ ). ESI-MS:  $m/z$  207.3 [ $M$  +  $H$ ] $^+$ , 224.4 [ $M$  +  $NH_4$ ] $^+$ ,  $C_8H_{14}O_4S$  (206.06).

#### 4.1.2. Synthesis of methyl 3-oxotetrahydro-2H-thiopyran-2-carboxylate (**10**)

To a solution of sodium hydride (60% in mineral oil, 0.06 g, 1.5 mmol) in THF (10 mL) was slowly added the intermediate **9** (0.21 g, 1.0 mmol) in 2 mL of THF at –10 °C under a nitrogen atmosphere, and the mixture was stirred at room temperature for 2 h. Then the reaction solution was acidified to pH 7 with diluted hydrochloric acid and extracted with EtOAc (3  $\times$  10 mL). The combined organic layer was washed with saturated brine (3  $\times$  5 mL), dried over anhydrous  $Na_2SO_4$ , filtered, and concentrated in vacuum to give intermediate **10** as a yellow oil and was used in next step without purification. Yield: 76%. ESI-MS:  $m/z$  175.3 [ $M$  +  $H$ ] $^+$ , 192.5 [ $M$  +  $NH_4$ ] $^+$ ,  $C_7H_{10}O_3S$  (174.04).

#### 4.1.3. Synthesis of 2-(methylthio)-7,8-dihydro-6H-thiopyrano[3,2-*d*]pyrimidin-4-ol (**11**)

To a solution of potassium hydroxide (0.11 g, 2.0 mmol) in MeOH (10 mL) was added the intermediate **10** (0.17 g, 1.0 mmol) and S-methylthiuronium sulfate (0.29 g, 1.5 mmol), and the mixture was stirred at room temperature for 8 h. Then water (50 mL) and HOAc (1.0 mL) were added to the reaction mixture. The resulting precipitate was collected by filtration, washed with water (3  $\times$  5 mL), and dried to provide intermediate **11** as a white solid. Yield: 80%, mp: 234–236 °C.  $^1H$  NMR (400 MHz, DMSO- $d_6$ ):  $\delta$  12.70 (s, 1H, OH), 2.94–2.84 (m, 2H,  $C_6$ -dihydrothiopyranopyrimidine-H), 2.61 (t,  $J$  = 6.3 Hz, 2H,  $C_8$ -dihydrothiopyranopyrimidine-H), 2.45 (s, 3H,  $CH_3$ ), 2.08–1.95 (m, 2H,  $C_7$ -dihydrothiopyranopyrimidine-H). ESI-MS:  $m/z$  215.4 [ $M$  +  $H$ ] $^+$ , 237.3 [ $M$  +  $Na$ ] $^+$ ,  $C_8H_{10}N_2OS_2$  (214.02).

#### 4.1.4. Synthesis of 7,8-dihydro-6H-thiopyrano[3,2-d]pyrimidine-2,4-diol (**12**)

Intermediate **11** (0.21 g, 1.0 mmol) was suspended in a solution of H<sub>2</sub>O (10 mL) and HOAc (5.0 mL), and then the mixture was heated to reflux for 24 h. After cooling to room temperature, the resulting precipitate was collected by filtration, washed with water (3 × 5 mL), and dried to afford intermediate **12** as a colorless crystalline solid. Yield: 52%, mp: >300 °C. <sup>1</sup>H NMR (400 MHz, DMSO-*d*<sub>6</sub>): δ 11.17 (s, 1H, C<sub>4</sub>-OH), 10.82 (s, 1H, C<sub>2</sub>-OH), 2.84 (d, *J* = 6.0 Hz, 2H, C<sub>6</sub>-dihydrothiopyranopyrimidine-H), 2.43 (t, *J* = 6.3 Hz, 2H, C<sub>8</sub>-dihydrothiopyranopyrimidine-H), 2.04–1.91 (m, 2H, C<sub>7</sub>-dihydrothiopyranopyrimidine-H). ESI-MS: *m/z* 185.0 [M + H]<sup>+</sup>, 207.2 [M + Na]<sup>+</sup>, C<sub>7</sub>H<sub>8</sub>N<sub>2</sub>O<sub>2</sub>S (184.03).

#### 4.1.5. Synthesis of 2,4-dichloro-7,8-dihydro-6H-thiopyrano[3,2-d]pyrimidine (**13**)

Intermediate **12** (0.18 g, 1.0 mmol) and *N,N*-dimethylaniline (0.03 g, 0.25 mmol) were dissolved in 10 mL of POCl<sub>3</sub> and then the mixture was refluxed at 110 °C for 12 h. After cooling to room temperature, the reaction solution was slowly added to ice and filtered. The crude precipitate was further purified by silica gel column chromatography with EtOAc:PE (1:8) as the eluent to provide intermediate **13** as a white solid. Yield: 69%, mp: 105–107 °C. ESI-MS: *m/z* 221.3 [M + H]<sup>+</sup>, C<sub>7</sub>H<sub>6</sub>Cl<sub>2</sub>N<sub>2</sub>S (219.96).

#### 4.1.6. General procedure for the synthesis of intermediates **14a–c**

To a solution of intermediate **13** (0.22 g, 1.0 mmol) and potassium carbonate (0.28 g, 2.0 mmol) in DMF (5 mL), the different material 4-hydroxy-3,5-dimethylbenzoxonitrile (0.14 g, 1.0 mmol) or (*E*)-3-(4-hydroxy-3,5-dimethylphenyl)acrylonitrile (0.17 g, 1.0 mmol) or 2,4,6-trimethylphenol (0.14 g, 1.0 mmol) was added and stirred at room temperature for 6 h. Then the reaction mixture was poured into water (20 mL) and extracted with EtOAc (3 × 10 mL). The combined organic layer was washed with saturated brine (3 × 5 mL), dried over anhydrous Na<sub>2</sub>SO<sub>4</sub>, filtered, and finally purified by silica gel column chromatography with EtOAc:PE (1:6) as the eluent to give the corresponding intermediates **14a–c** as a white solid.

4.1.6.1. 4-((2-Chloro-7,8-dihydro-6H-thiopyrano[3,2-d]pyrimidin-4-yl)oxy)-3,5-dimethylbenzoxonitrile (**14a**). White solid, yield: 67%, mp: 254–256 °C. <sup>1</sup>H NMR (400 MHz, DMSO-*d*<sub>6</sub>): δ 7.73 (s, 2H, C<sub>3</sub>,C<sub>5</sub>-Ph-H), 3.16 (d, *J* = 5.6 Hz, 2H, C<sub>6</sub>-dihydrothiopyranopyrimidine-H), 2.92 (t, *J* = 6.2 Hz, 2H, C<sub>8</sub>-dihydrothiopyranopyrimidine-H), 2.23–2.13 (m, 2H, C<sub>7</sub>-dihydrothiopyranopyrimidine-H), 2.07 (s, 6H, CH<sub>3</sub> × 2). ESI-MS: *m/z* 332.4 [M + H]<sup>+</sup>, C<sub>16</sub>H<sub>14</sub>ClN<sub>3</sub>OS (331.05).

4.1.6.2. (*E*)-3-(4-((2-Chloro-7,8-dihydro-6H-thiopyrano[3,2-d]pyrimidin-4-yl)oxy)-3,5-dimethylphenyl)acrylonitrile (**14b**). White solid, yield: 86%, mp: 240–242 °C. <sup>1</sup>H NMR (400 MHz, DMSO-*d*<sub>6</sub>): δ 7.34 (d, *J* = 16.7 Hz, 1H, ArCH = ), 7.19 (s, 2H, C<sub>3</sub>,C<sub>5</sub>-Ph-H), 5.82 (d, *J* = 16.6 Hz, 1H, =CHCN), 3.17–3.05 (m, 2H, C<sub>6</sub>-dihydrothiopyranopyrimidine-H), 2.97 (t, *J* = 6.3 Hz, 2H, C<sub>8</sub>-dihydrothiopyranopyrimidine-H), 2.30 (p, *J* = 6.2 Hz, 2H, C<sub>7</sub>-dihydrothiopyranopyrimidine-H), 2.13 (s, 6H, CH<sub>3</sub> × 2). ESI-MS: *m/z* 358.3 [M + H]<sup>+</sup>, C<sub>18</sub>H<sub>16</sub>ClN<sub>3</sub>OS (357.07).

4.1.6.3. 2-Chloro-4-(mesityloxy)-7,8-dihydro-6H-thiopyrano[3,2-d]pyrimidine (**14c**). White solid, yield: 73%, mp:

176–178 °C. ESI-MS: *m/z* 321.4 [M + H]<sup>+</sup>, C<sub>16</sub>H<sub>17</sub>ClN<sub>2</sub>OS (320.08).

#### 4.1.7. General procedure for the synthesis of target compounds **15a** and **15b**

BINAP (0.03 g, 0.05 mmol) and Pd<sub>2</sub>(dba)<sub>3</sub> (0.05 g, 0.05 mmol) were first suspended in 1,4-dioxane (20 mL) under stirring at room temperature for 15 min. Then the 4-aminobenzonitrile (0.11 g, 0.9 mol) and cesium carbonate (0.97 g, 3.0 mol) were added and the stir was continued for another 10 min. Finally, intermediate **14a** (0.33 g, 1.0 mmol) or **14b** (0.36 g, 1.0 mmol) was added. The mixture was backfilled with nitrogen fully and heated at 100 °C for 12 h. After cooling to room temperature, the reaction solution was filtered, and the obtained organic layer was purified by silica gel column chromatography with EtOAc:PE (1:4) as the eluent and finally recrystallized from EtOAc–PE to afford the target compounds **15a** or **15b** as a white solid.

4.1.7.1. 4-((2-((4-Cyanophenyl)amino)-7,8-dihydro-6H-thiopyrano[3,2-d]pyrimidin-4-yl)oxy)-3,5-dimethylbenzoxonitrile (**15a**). White solid, yield: 77%, mp: 253–255 °C. <sup>1</sup>H NMR (400 MHz, DMSO-*d*<sub>6</sub>): δ 9.98 (s, 1H, NH), 7.78 (s, 2H, C<sub>3</sub>,C<sub>5</sub>-Ph'-H), 7.45 (s, 4H, C<sub>2</sub>,C<sub>3</sub>,C<sub>5</sub>,C<sub>6</sub>-Ph'-H), 3.19–3.05 (m, 2H, C<sub>6</sub>-dihydrothiopyranopyrimidine-H), 2.88 (t, *J* = 6.2 Hz, 2H, C<sub>8</sub>-dihydrothiopyranopyrimidine-H), 2.26–2.16 (m, 2H, C<sub>7</sub>-dihydrothiopyranopyrimidine-H), 2.11 (s, 6H, CH<sub>3</sub> × 2). <sup>13</sup>C NMR (100 MHz, DMSO-*d*<sub>6</sub>): δ 163.63, 163.07, 154.68, 154.12, 145.20, 133.10, 133.02, 132.98, 119.92, 119.00, 118.05, 109.09, 104.50, 102.39, 31.74, 26.34, 22.96, 16.12. ESI-MS: *m/z* 414.5 [M + H]<sup>+</sup>, 431.5 [M + NH<sub>4</sub>]<sup>+</sup>. C<sub>23</sub>H<sub>19</sub>N<sub>5</sub>OS (413.13). HPLC purity: 98.54%.

4.1.7.2. (*E*)-4-((4-(2-Cyanovinyl)-2,6-dimethylphenoxy)-7,8-dihydro-6H-thiopyrano[3,2-d]pyrimidin-2-yl)amino)benzoxonitrile (**15b**). White solid, yield: 61%, mp: 278–280 °C. <sup>1</sup>H NMR (400 MHz, DMSO-*d*<sub>6</sub>): δ 9.95 (s, 1H, NH), 7.68 (d, *J* = 16.7 Hz, 1H, ArCH = ), 7.54 (s, 2H, C<sub>3</sub>,C<sub>5</sub>-Ph'-H), 7.48 (d, *J* = 8.6 Hz, 2H, C<sub>3</sub>,C<sub>5</sub>-Ph'-H), 7.39 (d, *J* = 8.8 Hz, 2H, C<sub>2</sub>,C<sub>6</sub>-Ph'-H), 6.48 (d, *J* = 16.7 Hz, 1H, =CHCN), 3.19–3.06 (m, 2H, C<sub>6</sub>-dihydrothiopyranopyrimidine-H), 2.87 (t, *J* = 6.2 Hz, 2H, C<sub>8</sub>-dihydrothiopyranopyrimidine-H), 2.20 (p, *J* = 6.0 Hz, 2H, C<sub>7</sub>-dihydrothiopyranopyrimidine-H), 2.08 (s, 6H, CH<sub>3</sub> × 2). <sup>13</sup>C NMR (100 MHz, DMSO-*d*<sub>6</sub>): δ 163.47, 163.30, 154.76, 152.47, 150.45, 145.29, 132.97, 131.93, 131.63, 128.64, 119.95, 119.33, 118.06, 104.49, 102.26, 96.93, 31.71, 26.33, 22.98, 16.40. ESI-MS: *m/z* 440.6 [M + H]<sup>+</sup>, 457.6 [M + NH<sub>4</sub>]<sup>+</sup>, C<sub>25</sub>H<sub>21</sub>N<sub>5</sub>OS (439.15). HPLC purity: 96.28%.

#### 4.1.8. General procedure for the synthesis of target compounds **16a** and **16b**

A mixture of compound **15a** (0.41 g, 1.0 mmol) and 3-chloroperbenzoic acid (0.20 g, 1.2 mmol) in DCM (10 mL) was stirred at –78 °C or room temperature for 6 h. Then saturated sodium bisulfite solution (10 mL) was added and extracted with DCM (3 × 10 mL). The combined organic layer was washed with saturated brine (3 × 5 mL), dried over anhydrous Na<sub>2</sub>SO<sub>4</sub>, filtered, purified by silica gel column chromatography with EtOAc:PE (1:4) as the eluent, and finally recrystallized from EtOAc–PE to give the target compounds **16a** or **16b** as a white solid.

4.1.8.1. 4-((2-((4-Cyanophenyl)amino)-5-oxido-7,8-dihydro-6H-thiopyrano[3,2-d]pyrimidin-4-yl)oxy)-3,5-

*dimethylbenzotrile (16a)*. White solid, yield: 72%, mp: 247–249 °C. <sup>1</sup>H NMR (400 MHz, DMSO-*d*<sub>6</sub>): δ 10.52 (s, 1H, NH), 7.80 (d, *J* = 4.6 Hz, 2H, C<sub>3</sub>,C<sub>5</sub>-Ph''-H), 7.50 (s, 4H, C<sub>2</sub>,C<sub>3</sub>,C<sub>5</sub>,C<sub>6</sub>-Ph'-H), 3.32–3.19 (m, 2H, C<sub>8</sub>-dihydrothiopyranopyrimidine-H), 3.09–2.79 (m, 2H, C<sub>6</sub>-dihydrothiopyranopyrimidine-H), 2.61–2.51 (m, 2H, C<sub>7</sub>-dihydrothiopyranopyrimidine-H), 2.15 (d, *J* = 14.7 Hz, 6H, CH<sub>3</sub> × 2). <sup>13</sup>C NMR (100 MHz, DMSO-*d*<sub>6</sub>): δ 169.09, 167.61, 158.94, 153.63, 144.12, 133.16, 133.08, 119.60, 119.31, 118.95, 111.11, 109.44, 104.19, 60.21, 45.19, 32.08, 16.22, 12.89. ESI-MS: *m/z* 447.5 [M + NH<sub>4</sub>]<sup>+</sup>, 452.3 [M + Na]<sup>+</sup>, C<sub>23</sub>H<sub>19</sub>N<sub>5</sub>O<sub>2</sub>S (429.13). HPLC purity: 99.31%.

4.1.8.2. 4-((2-((4-Cyanophenyl)amino)-5,5-dioxido-7,8-dihydro-6H-thiopyrano[3,2-*d*]pyrimidin-4-yl)oxy)-3,5-dimethylbenzotrile (**16b**). White solid, yield: 62%, mp: 263–265 °C. <sup>1</sup>H NMR (400 MHz, DMSO-*d*<sub>6</sub>): δ 10.62 (s, 1H, NH), 7.81 (s, 2H, C<sub>3</sub>,C<sub>5</sub>-Ph''-H), 7.64–7.18 (m, 4H, C<sub>2</sub>,C<sub>3</sub>,C<sub>5</sub>,C<sub>6</sub>-Ph'-H), 3.69–3.55 (m, 2H, C<sub>6</sub>-dihydrothiopyranopyrimidine-H), 3.02 (t, *J* = 6.0 Hz, 2H, C<sub>8</sub>-dihydrothiopyranopyrimidine-H), 2.34 (d, *J* = 5.1 Hz, 2H, C<sub>7</sub>-dihydrothiopyranopyrimidine-H), 2.16 (s, 6H, CH<sub>3</sub> × 2). <sup>13</sup>C NMR (100 MHz, DMSO-*d*<sub>6</sub>): δ 169.89, 164.70, 158.49, 153.31, 143.82, 133.19, 133.08, 132.92, 119.52, 119.44, 118.92, 112.61, 109.52, 104.48, 52.49, 32.08, 18.98, 16.08. ESI-MS: *m/z* 463.5 [M + NH<sub>4</sub>]<sup>+</sup>, 468.4 [M + Na]<sup>+</sup>, C<sub>23</sub>H<sub>19</sub>N<sub>5</sub>O<sub>3</sub>S (445.12). HPLC purity: 95.98%.

#### 4.1.9. General procedure for the synthesis of intermediates **18a** and **18b**

A mixture of intermediate **14a** (0.33 g, 1.0 mmol), *tert*-butyl piperazine-1-carboxylate (0.23 g, 1.2 mmol), or *tert*-butyl piperidin-4-ylcarbamate (0.24 g, 1.2 mmol), and potassium carbonate (0.28 g, 2.0 mmol) in 10 mL of DMF was heated at 120 °C for 12 h. After cooling to room temperature, the reaction solution was added to the 50 mL of water. The resulting precipitate was collected by filtration, washed with water (3 × 5 mL), and dried to provide crude products **17a** or **17b**, which was used directly in the next step without further purification. Subsequently, to a solution of **17a** (0.48 g, 1.0 mmol) or **17b** (0.50 g, 1.0 mmol) in DCM (10 mL) was added trifluoroacetic acid (1.14 g, 10 mmol) and the mixture was stirred at room temperature for 4 h. Then the reaction solution was alkalinized to pH 9 with saturated sodium bicarbonate solution and extracted with DCM (3 × 10 mL). The combined organic layer was washed with saturated brine (3 × 5 mL), dried over anhydrous Na<sub>2</sub>SO<sub>4</sub>, filtered, and finally purified by silica gel column chromatography with MeOH:DCM (1:10) as the eluent to afford the intermediates **18a** or **18b** as a white solid.

4.1.9.1. 3,5-Dimethyl-4-((2-(piperazin-1-yl)-7,8-dihydro-6H-thiopyrano[3,2-*d*]pyrimidin-4-yl)oxy)benzotrile (**18a**). White solid, yield: 52%. <sup>1</sup>H NMR (400 MHz, DMSO-*d*<sub>6</sub>): δ 8.83 (s, 1H, piperazine-NH), 7.69 (s, 2H, C<sub>3</sub>,C<sub>5</sub>-Ph-H), 3.53 (t, *J* = 5.1 Hz, 4H, C<sub>2</sub>,C<sub>6</sub>-piperazine-H), 3.12–2.94 (m, 6H, C<sub>6</sub>-dihydrothiopyranopyrimidine-H, C<sub>3</sub>,C<sub>5</sub>-piperazine-H), 2.77 (t, *J* = 6.3 Hz, 2H, C<sub>8</sub>-dihydrothiopyranopyrimidine-H), 2.21–2.10 (m, 2H, C<sub>7</sub>-dihydrothiopyranopyrimidine-H), 2.08 (s, 6H, CH<sub>3</sub> × 2). <sup>13</sup>C NMR (100 MHz, DMSO-*d*<sub>6</sub>): δ 170.78, 163.31, 157.15, 153.73, 132.86, 119.18, 108.83, 101.57, 42.65, 41.11, 32.03, 26.31, 23.18, 21.22, 16.15. C<sub>20</sub>H<sub>23</sub>N<sub>5</sub>OS (381.16).

4.1.9.2. 4-((2-(4-Aminopiperidin-1-yl)-7,8-dihydro-6H-thiopyrano[3,2-*d*]pyrimidin-4-yl)oxy)-3,5-dimethylbenzotrile

(**18b**). White solid, yield: 64%, mp: 234–236 °C. <sup>1</sup>H NMR (400 MHz, DMSO-*d*<sub>6</sub>): δ 7.87 (s, 2H, NH<sub>2</sub>), 7.69 (s, 2H, C<sub>3</sub>,C<sub>5</sub>-Ph-H), 4.11 (d, *J* = 13.2 Hz, 2H, piperidine-H), 3.20 (tt, *J* = 11.0, 3.9 Hz, 1H, piperidine-H), 3.10–3.01 (m, 2H, C<sub>6</sub>-dihydrothiopyranopyrimidine-H), 2.80–2.66 (m, 4H, piperidine-H, C<sub>8</sub>-dihydrothiopyranopyrimidine-H), 2.14 (p, *J* = 6.1 Hz, 2H, C<sub>7</sub>-dihydrothiopyranopyrimidine-H), 2.08 (s, 6H, CH<sub>3</sub> × 2), 1.78 (d, *J* = 12.0 Hz, 2H, piperidine-H), 1.25 (tt, *J* = 13.1, 6.6 Hz, 2H, piperidine-H). C<sub>21</sub>H<sub>25</sub>N<sub>5</sub>OS (395.18).

#### 4.1.10. General procedure for the synthesis of target compounds **19a** and **19b**

Intermediate **18a** (0.38 g, 1.0 mmol) or **18b** (0.40 g, 1.0 mmol) was dissolved in 10 mL of DMF, followed by the addition of 4-(bromomethyl)benzenesulfonamide (0.28 g, 1.1 mmol) and potassium carbonate (0.17 g, 1.2 mmol). After being stirred at room temperature until completion, the reaction mixture was poured into water (20 mL) and extracted with EtOAc (3 × 10 mL). The combined organic layer was washed with saturated brine (3 × 5 mL), dried over anhydrous Na<sub>2</sub>SO<sub>4</sub>, filtered, purified by silica gel column chromatography with MeOH:DCM (1:20) as the eluent, and finally recrystallized from EtOAc–PE to give the target compounds **19a** or **19b** as a white solid.

4.1.10.1. 4-((4-(4-(4-Cyano-2,6-dimethylphenoxy)-7,8-dihydro-6H-thiopyrano[3,2-*d*]pyrimidin-2-yl)piperazin-1-yl)methyl)benzenesulfonamide (**19a**). White solid, yield: 60%, mp: 141–143 °C. <sup>1</sup>H NMR (400 MHz, DMSO-*d*<sub>6</sub>): δ 7.77 (d, *J* = 8.3 Hz, 2H, C<sub>3</sub>,C<sub>5</sub>-Ph'-H), 7.66 (s, 2H, C<sub>3</sub>,C<sub>5</sub>-Ph''-H), 7.46 (d, *J* = 8.3 Hz, 2H, C<sub>2</sub>,C<sub>6</sub>-Ph'-H), 7.32 (s, 2H, SO<sub>2</sub>NH<sub>2</sub>), 3.50 (s, 2H, N–CH<sub>2</sub>), 3.36 (s, 4H, C<sub>2</sub>,C<sub>6</sub>-piperazine-H), 3.11–2.98 (m, 2H, C<sub>6</sub>-dihydrothiopyranopyrimidine-H), 2.73 (dt, *J* = 178.4, 6.2 Hz, 2H, C<sub>8</sub>-dihydrothiopyranopyrimidine-H), 2.27 (t, *J* = 4.5 Hz, 4H, C<sub>3</sub>,C<sub>5</sub>-piperazine-H), 2.19–2.09 (m, 2H, C<sub>7</sub>-dihydrothiopyranopyrimidine-H), 2.07 (s, 6H, CH<sub>3</sub> × 2). <sup>13</sup>C NMR (100 MHz, DMSO-*d*<sub>6</sub>): δ 163.23, 163.02, 157.57, 153.89, 143.26, 142.61, 132.90, 132.73, 129.57, 126.08, 119.10, 108.69, 100.06, 61.70, 52.51, 43.83, 32.05, 26.32, 23.34, 16.18. ESI-MS: *m/z* 551.2 [M + H]<sup>+</sup>, C<sub>27</sub>H<sub>30</sub>N<sub>6</sub>O<sub>3</sub>S<sub>2</sub> (550.18). HPLC purity: 96.60%.

4.1.10.2. 4-((1-(4-(4-Cyano-2,6-dimethylphenoxy)-7,8-dihydro-6H-thiopyrano[3,2-*d*]pyrimidin-2-yl)piperidin-4-yl)amino)benzenesulfonamide (**19b**). White solid, yield: 66%, mp: 227–229 °C. <sup>1</sup>H NMR (400 MHz, DMSO-*d*<sub>6</sub>): δ 7.74 (d, *J* = 8.2 Hz, 2H, C<sub>3</sub>,C<sub>5</sub>-Ph'-H), 7.68 (s, 2H, C<sub>3</sub>,C<sub>5</sub>-Ph''-H), 7.49 (d, *J* = 8.2 Hz, 2H, C<sub>2</sub>,C<sub>6</sub>-Ph'-H), 7.29 (s, 2H, SO<sub>2</sub>NH<sub>2</sub>), 3.97 (d, *J* = 10.2 Hz, 2H, piperidine-H, NH–CH<sub>2</sub>), 3.76 (s, 2H, NH–CH<sub>2</sub>), 3.10–2.98 (m, 2H, C<sub>6</sub>-dihydrothiopyranopyrimidine-H), 2.82–2.64 (m, 4H, piperidine-H, C<sub>8</sub>-dihydrothiopyranopyrimidine-H), 2.13 (m, 4H, piperidine-H, C<sub>7</sub>-dihydrothiopyranopyrimidine-H), 2.07 (s, 6H, CH<sub>3</sub> × 2), 1.71 (d, *J* = 10.2 Hz, 2H, piperidine-H), 1.05 (q, *J* = 9.7 Hz, 2H, piperidine-H). <sup>13</sup>C NMR (100 MHz, DMSO-*d*<sub>6</sub>): δ 163.07, 157.56, 154.01, 146.12, 142.73, 132.96, 132.70, 128.57, 125.92, 119.13, 108.64, 99.33, 60.22, 53.75, 49.50, 42.58, 32.08, 31.81, 26.33, 23.41, 16.17. ESI-MS: *m/z* 565.2 [M + H]<sup>+</sup>, C<sub>28</sub>H<sub>32</sub>N<sub>6</sub>O<sub>3</sub>S<sub>2</sub> (564.20). HPLC purity: 98.13%.

#### 4.1.11. General procedure for the synthesis of target compounds **20a–d**

To a solution of intermediate **14a** (0.33 g, 1.0 mmol), **14b** (0.36 g, 1.0 mmol), or **14c** (0.32 g, 1.0 mmol) in 10 mL of NMP was

added 1-(2-aminoethyl)pyrimidine-2,4(1*H*,3*H*)-dione (0.17 g, 1.1 mmol) and *N,N*-diisopropylethylamine (0.26 g, 2.0 mmol), and the mixture was stirred at 120 °C for 12 h. After cooling to room temperature, the reaction mixture was poured into water (20 mL) and extracted with EtOAc (3 × 10 mL). The combined organic layer was washed with saturated brine (3 × 5 mL), dried over anhydrous Na<sub>2</sub>SO<sub>4</sub>, filtered, purified by silica gel column chromatography with EtOAc:PE (1:4) as the eluent, and finally recrystallized from EtOAc–PE to afford the target compounds **20a–c** as a white solid. Using a similar synthetic method with the intermediate **14a** (0.33 g, 1.0 mmol) and 2-morpholinoethan-1-amine (0.14 g, 1.1 mmol) as starting materials, the target compound **20d** was prepared as a white solid.

4.1.11.1. 4-((2-((2-(2,4-Dioxo-3,4-dihydropyrimidin-1(2*H*)-yl)ethyl)amino)-7,8-dihydro-6*H*-thiopyrano[3,2-*d*]pyrimidin-4-yl)oxy)-3,5-dimethylbenzonitrile (**20a**). White solid, yield: 25%, mp: 203–205 °C. <sup>1</sup>H NMR (400 MHz, DMSO-*d*<sub>6</sub>): δ 11.21 (d, *J* = 2.3 Hz, 1H, uracil-NH), 7.74 (s, 2H, C<sub>3</sub>,C<sub>5</sub>-Ph-H), 7.29 (s, 1H, C<sub>2</sub>-uracil-H), 6.93 (s, 1H, NH), 5.41 (s, 1H, C<sub>3</sub>-uracil-H), 3.69 (s, 2H, NH–CH<sub>2</sub>), 3.40 (s, 2H, N–CH<sub>2</sub>), 3.13–3.00 (m, 2H, C<sub>6</sub>-dihydrothiopyranopyrimidine-H), 2.74 (t, *J* = 6.2 Hz, 2H, C<sub>8</sub>-dihydrothiopyranopyrimidine-H), 2.21–2.15 (m, 2H, C<sub>7</sub>-dihydrothiopyranopyrimidine-H), 2.14 (s, 6H, CH<sub>3</sub> × 2). <sup>13</sup>C NMR (100 MHz, DMSO-*d*<sub>6</sub>): δ 164.26, 163.16, 158.49, 154.01, 151.33, 146.09, 132.99, 132.84, 119.09, 108.66, 100.59, 99.99, 79.64, 31.76, 26.34, 23.35, 16.16. ESI-MS: *m/z* 451.5 [M + H]<sup>+</sup>, 473.3 [M + Na]<sup>+</sup>, C<sub>22</sub>H<sub>22</sub>N<sub>6</sub>O<sub>3</sub>S (450.15). HPLC purity: 98.36%.

4.1.11.2. (*E*)-3-(4-((2-((2-(2,4-Dioxo-3,4-dihydropyrimidin-1(2*H*)-yl)ethyl)amino)-7,8-dihydro-6*H*-thiopyrano[3,2-*d*]pyrimidin-4-yl)oxy)-3,5-dimethylphenyl)acrylonitrile (**20b**). White solid, yield: 37%, mp: 283–285 °C. <sup>1</sup>H NMR (400 MHz, DMSO-*d*<sub>6</sub>): δ 11.15 (d, *J* = 7.7 Hz, 1H, uracil-NH), 7.59 (d, *J* = 16.3 Hz, 1H, ArCH = ), 7.45 (s, 2H, C<sub>3</sub>,C<sub>5</sub>-Ph-H), 6.86 (s, 2H, C<sub>2</sub>-uracil-H, NH), 6.41 (d, *J* = 16.7 Hz, 1H, =CHCN), 5.31 (d, *J* = 7.7 Hz, 1H, C<sub>3</sub>-uracil-H), 3.62 (s, 2H, NH–CH<sub>2</sub>), 3.17 (s, 2H, N–CH<sub>2</sub>), 3.05–2.96 (m, 2H, C<sub>6</sub>-dihydrothiopyranopyrimidine-H), 2.67 (t, *J* = 6.3 Hz, 2H, C<sub>8</sub>-dihydrothiopyranopyrimidine-H), 2.15–2.08 (m, 2H, C<sub>7</sub>-dihydrothiopyranopyrimidine-H), 2.05 (s, 6H, CH<sub>3</sub> × 2). <sup>13</sup>C NMR (100 MHz, DMSO-*d*<sub>6</sub>): δ 164.26, 163.56, 158.58, 152.37, 151.33, 150.48, 131.63, 131.51, 128.46, 119.40, 96.69, 31.76, 26.35, 23.38, 16.55, 16.44. ESI-MS: *m/z* 477.4 [M + H]<sup>+</sup>, 499.5 [M + Na]<sup>+</sup>, C<sub>24</sub>H<sub>24</sub>N<sub>6</sub>O<sub>3</sub>S (476.16). HPLC purity: 97.19%.

4.1.11.3. 1-(2-((4-(Mesityloxy)-7,8-dihydro-6*H*-thiopyrano[3,2-*d*]pyrimidin-2-yl)amino)ethyl)pyrimidine-2,4(1*H*,3*H*)-dione (**20c**). White solid, yield: 37%, mp: 223–225 °C. <sup>1</sup>H NMR (400 MHz, DMSO-*d*<sub>6</sub>): δ 11.15 (d, *J* = 7.7 Hz, 1H, uracil-NH), 6.91 (s, 4H, C<sub>3</sub>,C<sub>5</sub>-Ph-H, C<sub>2</sub>-uracil-H, NH), 5.31 (d, *J* = 7.7 Hz, 1H, C<sub>3</sub>-uracil-H), 3.61 (s, 2H, NH–CH<sub>2</sub>), 3.19 (s, 2H, N–CH<sub>2</sub>), 3.04–2.93 (m, 2H, C<sub>6</sub>-dihydrothiopyranopyrimidine-H), 2.66 (t, *J* = 6.1 Hz, 2H, C<sub>8</sub>-dihydrothiopyranopyrimidine-H), 2.24 (s, 3H, CH<sub>3</sub>), 2.09 (dt, *J* = 12.1, 6.1 Hz, 2H, C<sub>7</sub>-dihydrothiopyranopyrimidine-H), 1.98 (s, 6H, CH<sub>3</sub> × 2). <sup>13</sup>C NMR (100 MHz, DMSO-*d*<sub>6</sub>): δ 164.25, 163.91, 158.65, 151.34, 147.88, 134.65, 130.20, 129.39, 100.62, 100.00, 31.73, 26.32, 23.41, 20.82, 16.40. ESI-MS: *m/z* 440.6 [M + H]<sup>+</sup>, C<sub>22</sub>H<sub>25</sub>N<sub>5</sub>O<sub>3</sub>S (439.17). HPLC purity: 98.42%.

4.1.11.4. 3,5-Dimethyl-4-((2-((2-morpholinoethyl)amino)-7,8-dihydro-6*H*-thiopyrano[3,2-*d*]pyrimidin-4-yl)oxy)benzonitrile

(**20d**). White solid, yield: 68%, mp: 142–144 °C. <sup>1</sup>H NMR (400 MHz, DMSO-*d*<sub>6</sub>): δ 7.67 (s, 2H, C<sub>3</sub>,C<sub>5</sub>-Ph-H), 6.81 (s, 1H, NH), 3.49 (s, 4H, C<sub>3</sub>,C<sub>5</sub>-morpholine-H), 3.02 (t, *J* = 5.5, 4H, NH–CH<sub>2</sub>, C<sub>6</sub>-dihydrothiopyranopyrimidine-H), 2.69 (t, *J* = 6.2 Hz, 2H, C<sub>8</sub>-dihydrothiopyranopyrimidine-H), 2.51–2.14 (m, 8H, N–CH<sub>2</sub>, C<sub>2</sub>,C<sub>6</sub>-morpholine-H, C<sub>7</sub>-dihydrothiopyranopyrimidine-H), 2.08 (s, 6H, CH<sub>3</sub> × 2). <sup>13</sup>C NMR (100 MHz, DMSO-*d*<sub>6</sub>): δ 163.43, 163.26, 158.61, 154.11, 133.00, 132.77, 119.06, 108.56, 66.59, 57.69, 53.65, 40.68, 38.06, 31.82, 26.34, 23.45, 16.15. ESI-MS: *m/z* 426.2 [M + H]<sup>+</sup>, C<sub>22</sub>H<sub>27</sub>N<sub>5</sub>O<sub>2</sub>S (425.19). HPLC purity: 99.00%.

#### 4.1.12. General procedure for the synthesis of intermediates **22a–c**

A mixture of intermediate **14a** (0.33 g, 1.0 mmol), **14b** (0.36 g, 1.0 mmol), or **14c** (0.32 g, 1.0 mmol), *tert*-butyl 4-aminopiperidine-1-carboxylate (0.24 g, 1.2 mmol), and potassium carbonate (0.28 g, 2.0 mmol) in 10 mL of DMF was heated at 100 °C for 10 h. After cooling to room temperature, the reaction solution was added to the 50 mL of water. The resulting precipitate was collected by filtration, washed with water (3 × 5 mL), and dried to provide crude products **21a–c**, which were used directly in the next step without further purification. Subsequently, to a solution of **21a** (0.50 g, 1.0 mmol) or **21b** (0.52 g, 1.0 mmol) or **21c** (0.48 g, 1.0 mmol) in DCM (10 mL) was added trifluoroacetic acid (1.14 g, 10 mmol) and the mixture was stirred at room temperature for 4 h. Then the reaction solution was alkalinized to pH 9 with saturated sodium bicarbonate solution and extracted with DCM (3 × 10 mL). The combined organic layer was washed with saturated brine (3 × 5 mL), dried over anhydrous Na<sub>2</sub>SO<sub>4</sub>, filtered, and finally purified by silica gel column chromatography with MeOH:DCM (1:10) as the eluent to afford the intermediates **22a–c** as a white solid.

4.1.12.1. 3,5-Dimethyl-4-((2-(piperidin-4-ylamino)-7,8-dihydro-6*H*-thiopyrano[3,2-*d*]pyrimidin-4-yl)oxy)benzonitrile (**22a**). White solid, yield: 63%, mp: >250 °C. <sup>1</sup>H NMR (400 MHz, DMSO-*d*<sub>6</sub>): δ 9.00 (s, 1H, piperidine-NH), 7.67 (s, 2H, C<sub>3</sub>,C<sub>5</sub>-Ph-H), 7.02 (s, 1H, NH), 3.14 (d, *J* = 12.5 Hz, 2H, C<sub>6</sub>-dihydrothiopyranopyrimidine-H), 3.07–2.99 (m, 2H, C<sub>8</sub>-dihydrothiopyranopyrimidine-H), 2.71 (t, *J* = 6.3 Hz, 4H, piperidine-H), 2.18–2.09 (m, 2H, C<sub>7</sub>-dihydrothiopyranopyrimidine-H), 2.07 (s, 6H, CH<sub>3</sub> × 2), 1.81 (s, 2H, piperidine-H), 1.54 (s, 3H, piperidine-H). <sup>13</sup>C NMR (100 MHz, DMSO-*d*<sub>6</sub>): δ 163.27, 157.76, 154.08, 132.96, 132.77, 119.08, 108.60, 46.02, 41.99, 31.86, 28.05, 26.31, 23.39, 16.18. ESI-MS: *m/z* 396.4 [M + H]<sup>+</sup>, C<sub>21</sub>H<sub>25</sub>N<sub>5</sub>OS (395.18).

4.1.12.2. (*E*)-3-(3,5-Dimethyl-4-((2-(piperidin-4-ylamino)-7,8-dihydro-6*H*-thiopyrano[3,2-*d*]pyrimidin-4-yl)oxy)phenyl)acrylonitrile (**22b**). White solid, yield: 18%. ESI-MS: *m/z* 422.3 [M + H]<sup>+</sup>, C<sub>23</sub>H<sub>27</sub>N<sub>5</sub>OS (421.19).

4.1.12.3. 4-(Mesityloxy)-*N*-(piperidin-4-yl)-7,8-dihydro-6*H*-thiopyrano[3,2-*d*]pyrimidin-2-amine (**22c**). White solid, yield: 29%, mp: >290 °C. <sup>1</sup>H NMR (400 MHz, DMSO-*d*<sub>6</sub>): δ 8.91 (s, 1H, piperidine-NH), 6.90 (s, 3H, C<sub>3</sub>,C<sub>5</sub>-Ph-H, NH), 3.15 (d, *J* = 12.6 Hz, 2H, C<sub>6</sub>-dihydrothiopyranopyrimidine-H), 3.07–2.96 (m, 2H, C<sub>8</sub>-dihydrothiopyranopyrimidine-H), 2.69 (t, *J* = 6.3 Hz, 4H, piperidine-H), 2.24 (s, 3H, CH<sub>3</sub>), 2.12 (p, *J* = 5.9 Hz, 2H, C<sub>7</sub>-dihydrothiopyranopyrimidine-H), 1.98 (s, 6H, CH<sub>3</sub> × 2), 1.82 (s, 2H, piperidine-H), 1.54 (s, 3H, piperidine-H). <sup>13</sup>C NMR (100 MHz, DMSO-*d*<sub>6</sub>): δ 164.00, 157.90, 147.95, 134.59, 130.15,

129.29, 46.06, 42.15, 31.84, 28.14, 26.30, 23.45, 20.81, 16.44. ESI-MS:  $m/z$  385.5 [M + H]<sup>+</sup>, C<sub>21</sub>H<sub>28</sub>N<sub>4</sub>OS (384.20).

#### 4.1.13. General procedure for the synthesis of target compounds 23a–i

Intermediate **22a** (0.40 g, 1.0 mmol), **22b** (0.42 g, 1.0 mmol), or **22c** (0.38 g, 1.0 mmol) was dissolved in 10 mL of DMF, followed by the addition of substituted benzyl chloride (or bromide) (1.1 mmol) and potassium carbonate (0.17 g, 1.2 mmol). After being stirred at room temperature until completion, the reaction mixture was poured into water (20 mL) and extracted with EtOAc (3 × 10 mL). The combined organic layer was washed with saturated brine (3 × 5 mL), dried over anhydrous Na<sub>2</sub>SO<sub>4</sub>, filtered, purified by silica gel column chromatography with MeOH:DCM (1:20) as the eluent, and finally recrystallized from EtOAc–PE to give the target compounds **23a–i** as a white solid.

4.1.13.1. 4-((2-((1-(4-Cyanobenzyl)piperidin-4-yl)amino)-7,8-dihydro-6H-thiopyrano[3,2-*d*]pyrimidin-4-yl)oxy)-3,5-dimethylbenzonitrile (**23a**). White solid, yield: 81%, mp: 184–186 °C. <sup>1</sup>H NMR (400 MHz, DMSO-*d*<sub>6</sub>): δ 7.77 (d, *J* = 8.2 Hz, 2H, C<sub>3</sub>, C<sub>5</sub>-Ph'-H), 7.66 (s, 2H, C<sub>3</sub>, C<sub>5</sub>-Ph''-H), 7.47 (d, *J* = 8.1 Hz, 2H, C<sub>2</sub>, C<sub>6</sub>-Ph'-H), 6.89 (br, 1H, NH), 3.48 (s, 2H, N-CH<sub>2</sub>), 3.12–2.95 (m, 2H, C<sub>6</sub>-dihydrothiopyranopyrimidine-H), 2.69 (t, *J* = 6.3 Hz, 5H, C<sub>8</sub>-dihydrothiopyranopyrimidine-H, piperidine-H), 2.19–2.02 (m, 8H, CH<sub>3</sub> × 2, C<sub>7</sub>-dihydrothiopyranopyrimidine-H), 1.63 (s, 4H, piperidine-H), 1.32 (s, 2H, piperidine-H). <sup>13</sup>C NMR (100 MHz, DMSO-*d*<sub>6</sub>): δ 163.26, 158.00, 154.22, 145.26, 133.01, 132.66, 132.58, 129.87, 119.38, 119.10, 110.08, 108.56, 61.93, 52.59, 48.66, 31.84, 31.66, 26.33, 23.47, 16.16. ESI-MS:  $m/z$  511.6 [M + H]<sup>+</sup>, C<sub>29</sub>H<sub>30</sub>N<sub>6</sub>OS (510.22). HPLC purity: 95.65%.

4.1.13.2. 4-((2-((1-(3-Cyanobenzyl)piperidin-4-yl)amino)-7,8-dihydro-6H-thiopyrano[3,2-*d*]pyrimidin-4-yl)oxy)-3,5-dimethylbenzonitrile (**23b**). White solid, yield: 81%, mp: 164–166 °C. <sup>1</sup>H NMR (400 MHz, DMSO-*d*<sub>6</sub>): δ 7.72 (d, *J* = 7.6 Hz, 1H, C<sub>4</sub>-Ph'-H), 7.68 (s, 1H, C<sub>2</sub>-Ph'-H), 7.65 (s, 2H, C<sub>3</sub>, C<sub>5</sub>-Ph''-H), 7.62 (d, *J* = 7.8 Hz, 1H, C<sub>6</sub>-Ph'-H), 7.53 (t, *J* = 7.7 Hz, 1H, C<sub>5</sub>-Ph''-H), 6.87 (s, 1H, NH), 3.45 (s, 2H, N-CH<sub>2</sub>), 3.09–2.94 (m, 2H, C<sub>6</sub>-dihydrothiopyranopyrimidine-H), 2.69 (t, *J* = 6.3 Hz, 4H, C<sub>8</sub>-dihydrothiopyranopyrimidine-H, piperidine-H), 2.19–2.09 (m, 2H, C<sub>7</sub>-dihydrothiopyranopyrimidine-H), 2.09 (s, 1H, piperidine-H), 2.06 (s, 6H, CH<sub>3</sub> × 2), 1.63 (s, 4H, piperidine-H), 1.31 (s, 2H, piperidine-H). <sup>13</sup>C NMR (100 MHz, DMSO-*d*<sub>6</sub>): δ 163.26, 157.96, 154.22, 140.90, 134.02, 133.02, 132.68, 132.44, 131.22, 129.89, 119.34, 119.10, 111.65, 108.56, 61.46, 55.38, 52.49, 31.86, 31.64, 31.15, 26.33, 23.47, 21.52, 16.16. ESI-MS:  $m/z$  511.2 [M + H]<sup>+</sup>, C<sub>29</sub>H<sub>30</sub>N<sub>6</sub>OS (510.22). HPLC purity: 97.91%.

4.1.13.3. 4-((2-((1-(2-Cyanobenzyl)piperidin-4-yl)amino)-7,8-dihydro-6H-thiopyrano[3,2-*d*]pyrimidin-4-yl)oxy)-3,5-dimethylbenzonitrile (**23c**). White solid, yield: 78%, mp: 206–208 °C. <sup>1</sup>H NMR (400 MHz, DMSO-*d*<sub>6</sub>): δ 7.79 (d, *J* = 7.6 Hz, 1H, C<sub>3</sub>-Ph'-H), 7.70–7.61 (m, 3H, C<sub>3</sub>, C<sub>5</sub>-Ph''-H, C<sub>5</sub>-Ph'-H), 7.52 (d, *J* = 7.7 Hz, 1H, C<sub>4</sub>-Ph'-H), 7.46 (t, *J* = 7.6 Hz, 1H, C<sub>6</sub>-Ph'-H), 6.86 (s, 1H, NH), 3.56 (s, 2H, N-CH<sub>2</sub>), 3.10–2.94 (m, 2H, C<sub>6</sub>-dihydrothiopyranopyrimidine-H), 2.69 (t, *J* = 6.2 Hz, 4H, C<sub>8</sub>-dihydrothiopyranopyrimidine-H, piperidine-H), 2.17–2.09 (m, 2H, C<sub>7</sub>-dihydrothiopyranopyrimidine-H), 2.09 (s, 1H, piperidine-H), 2.06 (s, 6H, CH<sub>3</sub> × 2), 1.59 (s, 4H, piperidine-H), 1.30 (s, 2H, piperidine-H). <sup>13</sup>C NMR (100 MHz, DMSO-*d*<sub>6</sub>): δ 163.26, 158.00, 154.22, 142.82,

133.42, 133.41, 133.02, 132.69, 130.48, 128.36, 119.08, 118.11, 112.53, 108.57, 60.36, 60.22, 52.54, 31.88, 31.58, 31.19, 26.33, 23.47, 16.17, 14.56. ESI-MS:  $m/z$  511.3 [M + H]<sup>+</sup>, C<sub>29</sub>H<sub>30</sub>N<sub>6</sub>OS (510.22). HPLC purity: 97.36%.

4.1.13.4. 3-((4-((4-(4-Cyano-2,6-dimethylphenoxy)-7,8-dihydro-6H-thiopyrano[3,2-*d*]pyrimidin-2-yl)amino)piperidin-1-yl)methyl)benzenesulfonamide (**23d**). White solid, yield: 74%, mp: 170–172 °C. <sup>1</sup>H NMR (400 MHz, DMSO-*d*<sub>6</sub>): δ 7.74 (s, 1H, C<sub>2</sub>-Ph'-H), 7.71 (d, *J* = 7.4 Hz, 1H, C<sub>4</sub>-Ph'-H), 7.67 (s, 2H, C<sub>3</sub>, C<sub>5</sub>-Ph''-H), 7.51 (t, *J* = 7.5 Hz, 1H, C<sub>6</sub>-Ph'-H), 7.47 (d, *J* = 7.5 Hz, 1H, C<sub>5</sub>-Ph'-H), 7.36 (s, 2H, SO<sub>2</sub>NH<sub>2</sub>), 6.80 (s, 1H, NH), 3.46 (s, 2H, N-CH<sub>2</sub>), 3.02 (dd, *J* = 6.7, 4.1 Hz, 2H, C<sub>6</sub>-dihydrothiopyranopyrimidine-H), 2.69 (t, *J* = 6.1 Hz, 4H, C<sub>8</sub>-dihydrothiopyranopyrimidine-H, piperidine-H), 2.19–2.09 (m, 2H, C<sub>7</sub>-dihydrothiopyranopyrimidine-H), 2.08 (s, 1H, piperidine-H), 2.06 (s, 6H, CH<sub>3</sub> × 2), 1.66 (s, 4H, piperidine-H), 1.32 (s, 2H, piperidine-H). <sup>13</sup>C NMR (100 MHz, DMSO-*d*<sub>6</sub>): δ 163.25, 157.84, 154.22, 144.59, 144.09, 140.31, 133.01, 132.74, 132.47, 129.26, 125.92, 124.68, 119.13, 108.55, 62.05, 52.62, 49.07, 31.82, 31.65, 26.30, 23.45, 16.18. ESI-MS:  $m/z$  565.2 [M + H]<sup>+</sup>, C<sub>28</sub>H<sub>32</sub>N<sub>6</sub>O<sub>3</sub>S<sub>2</sub> (564.20). HPLC purity: 96.68%.

4.1.13.5. Ethyl 4-((4-((4-(4-cyano-2,6-dimethylphenoxy)-7,8-dihydro-6H-thiopyrano[3,2-*d*]pyrimidin-2-yl)amino)piperidin-1-yl)methyl)benzoate (**23e**). White solid, yield: 57%, mp: 181–183 °C. <sup>1</sup>H NMR (400 MHz, DMSO-*d*<sub>6</sub>): δ 7.91 (d, *J* = 8.1 Hz, 2H, C<sub>3</sub>, C<sub>5</sub>-Ph'-H), 7.65 (s, 2H, C<sub>3</sub>, C<sub>5</sub>-Ph''-H), 7.41 (d, *J* = 8.1 Hz, 2H, C<sub>2</sub>, C<sub>6</sub>-Ph'-H), 6.87 (br, 1H, NH), 4.30 (q, *J* = 7.1 Hz, 2H, CO<sub>2</sub>CH<sub>2</sub>CH<sub>3</sub>), 3.46 (s, 2H, N-CH<sub>2</sub>), 3.09–2.97 (m, 2H, C<sub>6</sub>-dihydrothiopyranopyrimidine-H), 2.69 (t, *J* = 6.2 Hz, 4H, C<sub>8</sub>-dihydrothiopyranopyrimidine-H, piperidine-H), 2.16–2.09 (m, 2H, C<sub>7</sub>-dihydrothiopyranopyrimidine-H), 2.09 (s, 1H, piperidine-H), 2.06 (s, 6H, CH<sub>3</sub> × 2), 1.60 (s, 4H, piperidine-H), 1.31 (t, *J* = 7.1 Hz, 5H, CO<sub>2</sub>CH<sub>2</sub>CH<sub>3</sub>, piperidine-H). <sup>13</sup>C NMR (100 MHz, DMSO-*d*<sub>6</sub>): δ 166.11, 163.26, 157.99, 154.24, 144.87, 141.04, 133.02, 132.74, 129.52, 129.29, 128.98, 119.10, 108.56, 62.16, 61.04, 56.50, 52.62, 31.88, 31.65, 31.16, 26.33, 23.47, 16.15, 14.66. ESI-MS:  $m/z$  558.6 [M + H]<sup>+</sup>, C<sub>31</sub>H<sub>35</sub>N<sub>5</sub>O<sub>3</sub>S (557.25). HPLC purity: 98.38%.

4.1.13.6. 4-((2-((1-(4-Aminobenzyl)piperidin-4-yl)amino)-7,8-dihydro-6H-thiopyrano[3,2-*d*]pyrimidin-4-yl)oxy)-3,5-dimethylbenzonitrile (**23f**). White solid, yield: 64%, mp: 169–171 °C. <sup>1</sup>H NMR (400 MHz, DMSO-*d*<sub>6</sub>): δ 7.66 (s, 2H, C<sub>3</sub>, C<sub>5</sub>-Ph''-H), 6.87 (d, *J* = 8.1 Hz, 2H, C<sub>2</sub>, C<sub>6</sub>-Ph'-H), 6.49 (d, *J* = 8.2 Hz, 2H, C<sub>3</sub>, C<sub>5</sub>-Ph'-H), 4.94 (s, 2H, NH<sub>2</sub>), 3.17 (s, 2H, N-CH<sub>2</sub>), 3.08–2.95 (m, 2H, C<sub>6</sub>-dihydrothiopyranopyrimidine-H), 2.68 (t, *J* = 6.1 Hz, 4H, C<sub>8</sub>-dihydrothiopyranopyrimidine-H, piperidine-H), 2.12 (d, *J* = 5.3 Hz, 2H, C<sub>7</sub>-dihydrothiopyranopyrimidine-H), 2.09 (s, 1H, piperidine-H), 2.05 (s, 6H, CH<sub>3</sub> × 2), 1.48 (s, 4H, piperidine-H), 1.23 (s, 2H, piperidine-H). <sup>13</sup>C NMR (100 MHz, DMSO-*d*<sub>6</sub>): δ 163.24, 158.03, 154.22, 147.95, 133.01, 132.65, 130.16, 125.66, 123.82, 119.11, 114.01, 108.55, 62.55, 52.39, 31.65, 26.31, 23.46, 21.24, 19.03, 16.16, 14.56. ESI-MS:  $m/z$  501.5 [M + H]<sup>+</sup>, C<sub>28</sub>H<sub>32</sub>N<sub>6</sub>OS (500.24). HPLC purity: 98.40%.

4.1.13.7. *N*-4-((4-((4-(4-cyano-2,6-dimethylphenoxy)-7,8-dihydro-6H-thiopyrano[3,2-*d*]pyrimidin-2-yl)amino)piperidin-1-yl)methyl)phenyl)methanesulfonamide (**23g**). White solid, yield: 17%, mp: 153–155 °C. <sup>1</sup>H NMR (400 MHz, DMSO-*d*<sub>6</sub>): δ 9.68 (s, 1H, NHSO<sub>2</sub>CH<sub>3</sub>), 7.66 (s, 2H, C<sub>3</sub>, C<sub>5</sub>-Ph''-H), 7.21 (d, *J* = 8.3 Hz, 2H, C<sub>3</sub>, C<sub>5</sub>-Ph'-H), 7.14 (d, *J* = 8.4 Hz, 2H, C<sub>2</sub>, C<sub>6</sub>-Ph'-H), 6.70

(br, 1H, NH), 3.32 (s, 2H, N-CH<sub>2</sub>), 3.07–2.99 (m, 2H, C<sub>6</sub>-dihydrothiopyranopyrimidine-H), 2.96 (s, 3H, NHSO<sub>2</sub>CH<sub>3</sub>), 2.69 (t, *J* = 6.3 Hz, 4H, C<sub>8</sub>-dihydrothiopyranopyrimidine-H, piperidine-H), 2.11 (t, *J* = 5.7 Hz, 2H, C<sub>7</sub>-dihydrothiopyranopyrimidine-H), 2.09 (s, 1H, piperidine-H), 2.06 (s, 6H, CH<sub>3</sub> × 2), 1.55 (s, 4H, piperidine-H), 1.23 (s, 2H, piperidine-H). <sup>13</sup>C NMR (100 MHz, DMSO-*d*<sub>6</sub>): δ 163.25, 137.49, 134.60, 133.01, 132.90, 132.77, 132.70, 130.12, 120.24, 119.13, 108.54, 100.98, 62.08, 52.56, 39.62, 36.25, 31.81, 31.63, 31.17, 26.30, 23.45, 16.16. ESI-MS: *m/z* 579.2 [M + H]<sup>+</sup>, C<sub>29</sub>H<sub>34</sub>N<sub>6</sub>O<sub>3</sub>S<sub>2</sub> (578.21). HPLC purity: 98.56%.

4.1.13.8. (*E*)-4-((4-((4-(2-Cyanovinyl)-2,6-dimethylphenoxy)-7,8-dihydro-6H-thiopyrano[3,2-*d*]pyrimidin-2-yl)amino)piperidin-1-yl)methyl)benzenesulfonamide (**23h**). White solid, yield: 64%, mp: 237–239 °C. <sup>1</sup>H NMR (400 MHz, DMSO-*d*<sub>6</sub>): δ 7.77 (d, *J* = 8.3 Hz, 2H, C<sub>3</sub>, C<sub>5</sub>-Ph'-H), 7.59 (d, *J* = 16.7 Hz, 1H, ArCH = ), 7.43 (s, 4H, C<sub>2</sub>, C<sub>6</sub>-Ph'-H, C<sub>3</sub>, C<sub>5</sub>-Ph''-H), 7.30 (s, 2H, SO<sub>2</sub>NH<sub>2</sub>), 6.66 (s, 1H, NH), 6.40 (d, *J* = 16.7 Hz, 1H, =CHCN), 3.43 (s, 2H, N-CH<sub>2</sub>), 3.08–2.95 (m, 2H, C<sub>6</sub>-dihydrothiopyranopyrimidine-H), 2.68 (t, *J* = 6.2 Hz, 4H, C<sub>8</sub>-dihydrothiopyranopyrimidine-H, piperidine-H), 2.15–2.09 (m, 2H, C<sub>7</sub>-dihydrothiopyranopyrimidine-H), 2.06 (s, 1H, piperidine-H), 2.03 (s, 6H, CH<sub>3</sub> × 2), 1.61 (s, 4H, piperidine-H), 1.32 (s, 2H, piperidine-H). <sup>13</sup>C NMR (100 MHz, DMSO-*d*<sub>6</sub>): δ 163.65, 158.05, 152.59, 150.58, 143.41, 143.14, 131.62, 131.45, 129.43, 128.33, 126.05, 119.42, 96.51, 62.02, 52.67, 49.07, 31.89, 31.68, 26.34, 23.50, 16.46. ESI-MS: *m/z* 591.2 [M + H]<sup>+</sup>, C<sub>30</sub>H<sub>34</sub>N<sub>6</sub>O<sub>3</sub>S<sub>2</sub> (590.21). HPLC purity: 98.59%.

4.1.13.9. 4-((4-((4-(Mesityloxy)-7,8-dihydro-6H-thiopyrano[3,2-*d*]pyrimidin-2-yl)amino)piperidin-1-yl)methyl)benzenesulfonamide (**23i**). White solid, yield: 44%, mp: 218–220 °C. <sup>1</sup>H NMR (400 MHz, DMSO-*d*<sub>6</sub>): δ 7.77 (d, *J* = 8.3 Hz, 2H, C<sub>3</sub>, C<sub>5</sub>-Ph'-H), 7.44 (d, *J* = 8.0 Hz, 2H, C<sub>2</sub>, C<sub>6</sub>-Ph'-H), 7.30 (s, 2H, SO<sub>2</sub>NH<sub>2</sub>), 6.88 (s, 2H, C<sub>3</sub>, C<sub>5</sub>-Ph''-H), 6.60 (s, 1H, NH), 3.45 (s, 2H, N-CH<sub>2</sub>), 3.08–2.91 (m, 2H, C<sub>6</sub>-dihydrothiopyranopyrimidine-H), 2.79–2.57 (m, 4H, C<sub>8</sub>-dihydrothiopyranopyrimidine-H, piperidine-H), 2.23 (s, 3H, CH<sub>3</sub>), 2.10 (dt, *J* = 11.8, 5.4 Hz, 2H, C<sub>7</sub>-dihydrothiopyranopyrimidine-H), 1.97 (s, 6H, CH<sub>3</sub> × 2), 1.72–1.47 (m, 2H, piperidine-H), 1.46–1.10 (m, 2H, piperidine-H). <sup>13</sup>C NMR (100 MHz, DMSO-*d*<sub>6</sub>): δ 163.97, 162.36, 158.15, 148.02, 143.36, 143.13, 134.49, 130.15, 129.42, 129.22, 126.03, 61.99, 52.65, 49.07, 31.86, 31.74, 26.33, 23.54, 20.80, 16.43. ESI-MS: *m/z* 554.5 [M + H]<sup>+</sup>, C<sub>28</sub>H<sub>35</sub>N<sub>5</sub>O<sub>3</sub>S<sub>2</sub> (553.22). HPLC purity: 96.82%.

#### 4.1.14. Synthesis of tert-butyl (1-(3-cyanophenyl)piperidin-4-yl) carbamate (**25a**)

A mixture of 3-fluorobenzonitrile (**24**, 0.12 g, 1.0 mmol), tert-butyl piperidin-4-ylcarbamate (0.24 g, 1.2 mmol), and potassium carbonate (0.28 g, 2.0 mmol) in 10 mL of DMF was heated at 120 °C for 10 h. After cooling to room temperature, the reaction solution was added to the 50 mL of water. The resulting precipitate was collected by filtration, washed with water (3 × 5 mL), and dried to provide intermediate **25a** as a white solid. Yield: 66%. ESI-MS: *m/z* 302.6 [M + H]<sup>+</sup>, C<sub>17</sub>H<sub>23</sub>N<sub>3</sub>O<sub>2</sub> (301.18).

#### 4.1.15. Synthesis of tert-butyl (1-(3-carbamoylphenyl)piperidin-4-yl)carbamate (**25b**)

To a solution of intermediate **25a** (0.30 g, 1.0 mmol) and sodium hydroxide (0.04 g, 1.0 mmol) in EtOH (10 mL), hydrogen peroxide (5 mL) was dropwise added in and stirred at 50 °C for

2 h. Then the reaction mixture was poured into water (10 mL) and extracted with EtOAc (3 × 10 mL). The combined organic layer was washed with saturated brine (3 × 5 mL), dried over anhydrous Na<sub>2</sub>SO<sub>4</sub>, filtered, and concentrated in vacuum to give intermediate **25b** as a white solid. Yield: 62%, mp: 191–193 °C. ESI-MS: *m/z* 320.2 [M + H]<sup>+</sup>, C<sub>17</sub>H<sub>25</sub>N<sub>3</sub>O<sub>3</sub> (319.19).

#### 4.1.16. General procedure for the synthesis of intermediates **26a** and **26b**

To a solution of **25a** (0.30 g, 1.0 mmol) or **25b** (0.32 g, 1.0 mmol) in DCM (10 mL) was added trifluoroacetic acid (1.14 g, 10 mmol) and the mixture was stirred at room temperature for 4 h. Then the reaction solution was alkalinized to pH 9 with saturated sodium bicarbonate solution and extracted with DCM (3 × 10 mL). The combined organic layer was washed with saturated brine (3 × 5 mL), dried over anhydrous Na<sub>2</sub>SO<sub>4</sub>, filtered, and concentrated in vacuum to provide intermediates 3-(4-aminopiperidin-1-yl) benzonitrile (**26a**) or 3-(4-aminopiperidin-1-yl)benzamide (**26b**) as a viscous oil and was used in next step without purification.

#### 4.1.17. General procedure for the synthesis of target compounds **27a** and **27b**

BINAP (0.03 g, 0.05 mmol) and Pd<sub>2</sub>(dba)<sub>3</sub> (0.05 g, 0.05 mmol) were first suspended in 1,4-dioxane (20 mL) under stirring at room temperature for 15 min. Then the intermediate **26a** (0.20 g, 1.0 mmol) or **26b** (0.22 g, 1.0 mmol) and cesium carbonate (0.97 g, 3.0 mmol) were added and the stir was continued for another 10 min. Finally, intermediate **14a** (0.33 g, 1.0 mmol) was added. The mixture was backfilled with nitrogen fully and heated at 100 °C for 12 h. After cooling to room temperature, the reaction solution was filtered, and the obtained organic layer was purified by silica gel column chromatography with MeOH:DCM (1:50) as the eluent and finally recrystallized from EtOAc–PE to afford the target compound **27a** or **27b** as a white solid.

4.1.17.1. 4-((2-((1-(3-Cyanophenyl)piperidin-4-yl)amino)-7,8-dihydro-6H-thiopyrano[3,2-*d*]pyrimidin-4-yl)oxy)-3,5-dimethylbenzonitrile (**27a**). White solid, yield: 43%, mp: 186–188 °C. <sup>1</sup>H NMR (400 MHz, DMSO-*d*<sub>6</sub>): δ 7.65 (s, 2H, C<sub>3</sub>, C<sub>5</sub>-Ph'-H), 7.34 (dd, *J* = 8.5, 7.4, 1H, C<sub>5</sub>-Ph'-H), 7.26 (s, 1H, C<sub>2</sub>-Ph'-H), 7.21 (d, *J* = 8.5 Hz, 1H, C<sub>4</sub>-Ph'-H), 7.09 (d, *J* = 7.4 Hz, 1H, C<sub>6</sub>-Ph'-H), 6.82 (br, 1H, NH), 3.67 (s, 3H, piperidine-H), 3.02 (p, 2H, C<sub>6</sub>-dihydrothiopyranopyrimidine-H), 2.70 (t, *J* = 6.0 Hz, 3H, C<sub>8</sub>-dihydrothiopyranopyrimidine-H, piperidine-H), 2.12 (t, *J* = 5.7 Hz, 2H, C<sub>7</sub>-dihydrothiopyranopyrimidine-H), 2.08 (s, 1H, piperidine-H), 2.07 (s, 6H, CH<sub>3</sub> × 2), 1.69 (s, 2H, piperidine-H), 1.35 (s, 2H, piperidine-H). <sup>13</sup>C NMR (100 MHz, DMSO-*d*<sub>6</sub>): δ 163.26, 157.91, 154.17, 151.25, 133.01, 132.73, 130.64, 121.53, 120.26, 119.84, 119.12, 118.11, 112.37, 108.58, 56.52, 47.19, 31.85, 31.16, 30.82, 26.31, 23.42, 18.98, 16.18. ESI-MS: *m/z* 497.2 [M + H]<sup>+</sup>, C<sub>28</sub>H<sub>28</sub>N<sub>6</sub>O<sub>3</sub> (496.20). HPLC purity: 97.17%.

4.1.17.2. 3-(4-((4-(4-Cyano-2,6-dimethylphenoxy)-7,8-dihydro-6H-thiopyrano[3,2-*d*]pyrimidin-2-yl)amino)piperidin-1-yl)benzamide (**27b**). White solid, yield: 35%, mp: 232–234 °C. <sup>1</sup>H NMR (400 MHz, DMSO-*d*<sub>6</sub>): δ 7.91 (s, 1H, C<sub>4</sub>-Ph'-H), 7.68 (s, 2H, C<sub>3</sub>, C<sub>5</sub>-Ph'-H), 7.38 (s, 1H, C<sub>5</sub>-Ph'-H), 7.29 (s, 1H, C<sub>2</sub>-Ph'-H), 7.25 (s, 2H, CONH<sub>2</sub>), 7.03 (d, *J* = 4.1 Hz, 1H, C<sub>6</sub>-Ph'-H), 6.73 (s, 1H, NH), 3.65 (s, 3H, piperidine-H), 3.03 (d, *J* = 5.4 Hz, 2H, C<sub>6</sub>-dihydrothiopyranopyrimidine-H), 2.72 (t, *J* = 6.3 Hz, 3H, C<sub>8</sub>-

dihydrothiopyranopyrimidine-H, piperidine-H), 2.13 (t,  $J = 5.7$  Hz, 2H, C<sub>7</sub>-dihydrothiopyranopyrimidine-H), 2.09 (s, 1H, piperidine-H), 2.09 (s, 6H, CH<sub>3</sub> × 2), 1.72 (s, 2H, piperidine-H), 1.42 (s, 2H, piperidine-H). <sup>13</sup>C NMR (100 MHz, DMSO-*d*<sub>6</sub>): δ 168.71, 163.27, 157.95, 154.18, 151.18, 135.40, 133.01, 132.75, 129.25, 119.11, 118.66, 117.98, 115.09, 108.58, 56.50, 48.06, 31.88, 31.16, 26.32, 23.46, 19.04, 16.21. ESI-MS:  $m/z$  515.2 [M + H]<sup>+</sup>, C<sub>28</sub>H<sub>30</sub>N<sub>6</sub>O<sub>2</sub>S (514.22). HPLC purity: 98.29%.

#### 4.2. *In vitro* anti-HIV assay

The anti-HIV activity and cytotoxicity of the target compounds were evaluated in MT-4 cells by using the 3-(4,5-dimethylthiazol-2-yl)-2,5-diphenyltetrazolium bromide (MTT) method. The MTT method is based on the HIV-induced cytopathogenic effect (CPE) and measures the degree of cell killing on HIV infection. Firstly, stock solutions (10 × final concentration) of test compounds were added in 25 μL volumes to two series of triplicate wells to allow simultaneous evaluation of their effects on mock- and HIV-infected cells. Serial 5-fold dilutions of test compounds were prepared directly in flat-bottomed 96-well microtiter trays by adding 100 μL medium to the 25 μL stock solution and transferring 25 μL of this solution to another well that contained 100 μL medium *via* a Biomek 3000 robot (Beckman Instruments, Fullerton, CA). Each sample contains

#### 4.3. HIV-1 RT inhibition assay

The HIV-1 RT inhibition assay was conducted with an RT assay kit (Roche, Basel, Switzerland) by using the ELISA method. All the reagents for performing the RT reaction came from the kit and the ELSIA procedures for the RT inhibition assay were conducted following the description in the kit protocol. Briefly, the reaction mixture containing HIV-1 RT, reconstituted template and viral nucleotides [digoxigenin (DIG)-dUTP, biotin-dUTP and dTTP] in the incubation buffer with or without inhibitors was incubated for 1 h at 37 °C. The reaction mixture was transferred to a streptavidine-coated microtiter plate (MTP) and incubated for 1 h at 37 °C. The biotin-labeled dNTPs that were incorporated into the cDNA chain in the presence of RT were bound to streptavidin. The unbound dNTPs were removed with washing buffer and anti-DIG-POD working solution was added to the MTPs. The DIG-labeled dNTPs incorporated in cDNA were bound to the anti-DIG-POD antibody after incubation for 1 h at 37 °C. The unbound anti-DIG-PODs were washed out and the peroxide substrate (ABTS) solution was added to the MTPs. A color reaction occurred during cleavage of the substrate catalyzed by POD. The absorbance of the sample was determined using a microtiter plate ELISA reader (Multiskan Sky, Waltham, MA, USA). The inhibition rate of the test compounds was calculated by Eq. (1)

$$\text{Inhibition (\%)} = \frac{(\text{OD value with RT but without inhibitors} - \text{OD value with RT and inhibitors}) / (\text{OD value with RT but without inhibitors} - \text{OD value without RT and inhibitors}) \times 100}{(1)}$$

untreated control HIV- and mock-infected cell samples. HIV-1 WT strain (IIB), HIV-1 resistant strains [K103N + Y181C (RES056), L100I, K103N, Y181C, Y188L, E138K, and F227L + V106A] stock (50 μL) at 100–300 CCID<sub>50</sub> (50% cell culture infectious dose) or culture medium was added to either the infected or mock-infected wells of the microtiter tray. Mock-infected cells were used to evaluate the effect of test compounds on normal cells to assess their cytotoxicity. Exponentially growing MT-4 cells were centrifuged for 5 min at 1000 rpm and the supernatant was discarded. The MT-4 cells were resuspended at 6 × 10<sup>5</sup> cells/mL and 50 μL volumes were transferred to the microtiter tray wells. After infecting the MT-4 cells for five days, the viability of mock- and HIV-infected cells was examined spectrophotometrically by the MTT method. The MTT method is based on the reduction of yellow-colored MTT (Acros Organics, Geel, Belgium) by mitochondrial dehydrogenase in metabolically active cells to a blue–purple formazan that can be measured spectrophotometrically. The absorbances were read in an eight-channel computer-controlled photometer (Infinite M1000, Tecan) at two wavelengths (540 nm and 690 nm). All data were calculated using the median absorbance value of three wells. The 50% cytotoxic concentration (CC<sub>50</sub>) was defined as the concentration of test compounds that reduces the viability of the mock-infected MT-4 cells by 50%. The 50% effective concentration (EC<sub>50</sub>) was defined as the concentration of test compounds that achieves 50% protection against the cytopathic effect of the virus in infected cells.

#### 4.4. Cytochrome P450 inhibition assay

Compound **23h** was incubated with human liver microsome and NADPH cofactor in the presence of various CYP substrates: phenacetin for CYP1A2, diclofenac for CYP2C9, *S*-mephenytoin for CYP2C19, dextromethorphan for CYP2D6, and midazolam for CYP3A4. Standard CYP enzyme inhibitors were also tested as positive controls. To begin, a working solution (100 × ) of the test compound **23h** and standard inhibitors was prepared. Then, 20 μL of substrate solution was added to the appropriate wells, while 20 μL of potassium phosphate buffer was added to the blank wells. Next, 2 μL of the test compound and positive control working solution was added to their respective wells. For the wells without inhibitors, 2 μL of solvent was added, and for the blank wells, 2 μL of potassium phosphate buffer was added. To prepare the microsome working solution (0.253 mg/mL), 0.114 mL of human liver microsomes was combined with 8.886 mL of potassium phosphate buffer. Next, 158 μL of the HLM working solution was added to all wells of the incubation plate. The plate was pre-warmed for 10 min in a 37 °C water bath. For the NADPH solution (10 mmol/L), 62 mg of NADPH cofactor was added to 6.0 mL of MgCl<sub>2</sub> buffer. Then, 20 μL of the NADPH cofactor was added to all incubation wells. The plate was mixed and incubated for 10 min in a 37 °C water bath. At the time point, the reaction should be terminated by adding 400 μL of a cold stop solution (containing 200 ng/mL tolbutamide and 200 ng/mL labetalol in ACN). The samples were then centrifuged at 4000 rpm for 20 min

to precipitate the protein. Next, 200  $\mu\text{L}$  of the supernatant was diluted with 100  $\mu\text{L}$  of water and shaken for 10 min before the LC–MS/MS analysis.

#### 4.5. *hERG channel inhibition assay*

The hERG channel inhibition of compound **23h** was determined in HEK293 cells with stably transfected with hERG cDNA. HEK293 cells expressing hERG were plated in F12 dishes for 24 h and maintained at 37 °C under 5%  $\text{CO}_2$ . A micropipette was drawn out from the borosilicate glass to give a tip resistance between 2 and 5  $\text{M}\Omega$ . For each trial, a single dish of cells was removed from the incubator, washed twice with ECS, and placed on the microscope. HEK293 cells in the exponential growth phase were collected and resuspended in ECS for later use. The whole-cell recordings were conducted with a commercially available patch-clamp amplifier. The HEK293 cells were placed on the microscope stage, and one cell in the recording tank was randomly selected for testing. The perfusion system was fixed on an inverted microscope stage, and the cells were continuously perfused with ECS. Tail currents were evoked once every 15 s by a 1275 ms,  $-50$  mV repolarizing pulse following a 850 ms,  $+60$  mV depolarizing pulse with a hold voltage of  $-80$  mV. The voltage protocol started with a 50 ms depolarization pulse of  $-50$  mV, which served as the baseline for calculating the peak tail current amplitude. Only stable cells with recording parameters exceeding the threshold were used in the experiments. The hERG currents were allowed to stabilize over a 3 min period under the condition that vehicle alone prior to test compound application. The cells were kept in the test solution until the peak tail current was stable ( $<5\%$  change) for about 3 sweeps. Peak tail amplitudes were then plotted as a function of the sweep number. Before testing the composite application, the average of the three peak tail currents in the steady state was taken as the control current amplitude. Four or five peak tail current measurements at the steady state after test compound application were averaged and used as the remaining current amplitude after inhibition by the test compound. hERG inhibition rate was calculated by Eq. (2):

$$\text{Inhibition (\%)} = [1 - (\text{Remaining current amplitude}) / (\text{Control current amplitude})] \times 100 \quad (2)$$

#### 4.6. *In vivo pharmacokinetics assay*

All animal treatments were performed strictly in accordance with the institutional guidelines of animal ethical and welfare, after gaining approval from the Medical Ethical Committee of Shandong University. Sprague–Dawley (SD) rats (180–200 g) were purchased from the animal experimental center of Shandong University and were randomly divided into two groups receiving oral administration (20 mg/kg) or intravenous administration (2 mg/kg). Research protocols complied strictly with the institutional guidelines. Compound **23h** and ETR were suspended in a mixture solution of PEG-400 and normal saline. Blood samples (200  $\mu\text{L}$  each time) of the intravenous group were collected at 2, 5, 15, 30 min, 1, 1.5, 2, 4, and 8 h after dosing, and blood samples (200  $\mu\text{L}$  each time) of the oral administration group were collected at 5, 15, 30 min, 1, 2, 4, 6, 8, 10, and 12 h after dosing. All the plasma samples were obtained by centrifugation at 8000 rpm for 8 min, and immediately stored at  $-80$  °C until analysis. LC–MS

analysis was used to determine the concentration of **23h** and ETR in plasma. Briefly, 50  $\mu\text{L}$  of plasma was added to 50  $\mu\text{L}$  of internal standard and 300  $\mu\text{L}$  of methanol in a 5 mL centrifugation tube. All blood samples were centrifuged in an Eppendorf 5415D centrifuge at  $3000\times g$  for 10 min and quantified by Agilent 1200 LC/MSD (Agilent, USA). The supernatant layer was collected and a 20  $\mu\text{L}$  aliquot was injected for LC–MS analysis. Standard curves for **23h** and ETR in blood were generated by the addition of various concentrations of **23h** and ETR together with an internal standard to blank plasma.

#### 4.7. *In vivo safety experiment*

All animal treatments were performed strictly in accordance with the institutional guidelines of animal ethical and welfare, after gaining approval from the Medical Ethical Committee of Shandong University. Kunming mice (15–19 g) were purchased from the animal experimental center of Shandong University. Research protocols complied strictly with the institutional guidelines. Compound **23h** was suspended in a mixture solution of PEG-400 and normal saline at the concentration of 100 mg/mL. All mice had been fasted for 12 h, and then the mice in the test group were administered intragastrically by gavage at a dose of 2000 mg/kg of **23h** on the first day. The death, abnormal behaviors, and body weight of these mice were monitored every day during the subsequent 7 days.

#### Acknowledgments

We gratefully acknowledge financial support from the National Natural Science Foundation of China (NSFC nos. 81973181 and 81903453), Science Foundation for Outstanding Young Scholars of Shandong Province (ZR2020JQ31, China), Science Foundation for Excellent Young Scholars of Shandong Province (ZR2020YQ61, China), Foreign Cultural and Educational Experts Project (GXL20200015001, China), China Postdoctoral Science Foundation (2022M721948), Shandong Province Natural Science Foundation for Youths (ZR2023QH217, China), Natural Science Foundation of Jiangsu Province (BK20230252, China), Qilu Young Scholars Program of Shandong University, and Taishan Scholar Program at Shandong Province. We thank K. Erven, K. Uyttersprot, and C. Heens for technical assistance with the anti-HIV assays.

#### Author contributions

Xinyong Liu, Peng Zhan, Dongwei Kang, and Zhao Wang as the supervisors conceived the project and supplied the financial support. Zhao Wang and Heng Zhang conducted the synthesis of compounds and supervised the drug-likeness evaluation experiment. Erik De Clercq and Christophe Pannecouque conducted and supervised the biological activity evaluation assay. Molecular docking and molecular dynamics simulation were performed by Zhen Gao and Zhao Wang. Zhao Wang, Heng Zhang, Zhen Gao, and Zihao Sang conducted the data analysis. Zhao Wang wrote and revised the manuscript.

#### Conflicts of interest

The authors declare no competing financial interest.



## Appendix A. Supporting information

Supporting data to this article can be found online at <https://doi.org/10.1016/j.apsb.2023.11.023>.

## References

1. The Lancet HIV. UNAIDS strategy aligns HIV priorities with development goals. *Lancet HIV* 2021;**8**:e245.
2. Engelman A, Cherepanov P. The structural biology of HIV-1: mechanistic and therapeutic insights. *Nat Rev Microbiol* 2012;**10**:279–90.
3. Fauci AS, Lane HC. Four decades of HIV/AIDS—much accomplished, much to do. *N Engl J Med* 2020;**383**:1–4.
4. Larsen KP, Mathiharan YK, Kappel K, Coey AT, Chen DH, Barrero D, et al. Architecture of an HIV-1 reverse transcriptase initiation complex. *Nature* 2018;**557**:118–22.
5. Zhan P, Pannecouque C, De Clercq E, Liu X. Anti-HIV drug discovery and development: current innovations and future trends. *J Med Chem* 2016;**59**:2849–78.
6. Li G, Wang Y, De Clercq E. Approved HIV reverse transcriptase inhibitors in the past decade. *Acta Pharm Sin B* 2022;**12**:1567–90.
7. Wang Z, Cherukupalli S, Xie M, Wang W, Jiang X, Jia R, et al. Contemporary medicinal chemistry strategies for the discovery and development of novel HIV-1 non-nucleoside reverse transcriptase inhibitors. *J Med Chem* 2022;**65**:3729–57.
8. Zhuang C, Pannecouque C, De Clercq E, Chen F. Development of non-nucleoside reverse transcriptase inhibitors (NNRTIs): our past twenty years. *Acta Pharm Sin B* 2020;**10**:961–78.
9. Blair HA. Dolutegravir/Rilpivirine: a review in HIV-1 infection. *Drugs* 2018;**78**:1741–50.
10. Markham A. Cabotegravir plus rilpivirine: first approval. *Drugs* 2020;**80**:915–22.
11. Swindells S, Andrade-Villanueva JF, Richmond GJ, Rizzardini G, Baumgarten A, Masia M, et al. Long-acting cabotegravir and rilpivirine for maintenance of HIV-1 suppression. *N Engl J Med* 2020;**382**:1112–23.
12. Ding L, Zhuang C, Chen F. Druggability modification strategies of the diarylpyrimidine-type non-nucleoside reverse transcriptase inhibitors. *Med Res Rev* 2021;**41**:1255–90.
13. Gu SX, Lu HH, Liu GY, Ju XL, Zhu YY. Advances in diarylpyrimidines and related analogues as HIV-1 nonnucleoside reverse transcriptase inhibitors. *Eur J Med Chem* 2018;**158**:371–92.
14. Seidman D, Weber S, Aaron E. Dapivirine vaginal ring for HIV-1 prevention. *N Engl J Med* 2017;**376**:995.
15. Baeten JM, Palanee-Phillips T, Mgodini NM, Mayo AJ, Szydlow DW, Ramjee G, et al. Safety, uptake, and use of a dapivirine vaginal ring for HIV-1 prevention in African women (HOPE): an open-label, extension study. *Lancet HIV* 2021;**8**:e87–95.
16. Cilento ME, Kirby KA, Sarafianos SG. Avoiding drug resistance in HIV reverse transcriptase. *Chem Rev* 2021;**121**:3271–96.
17. Beyrer C, Pozniak A. HIV drug resistance—an emerging threat to epidemic control. *N Engl J Med* 2017;**377**:1605–7.
18. Battini L, Bollini M. Challenges and approaches in the discovery of human immunodeficiency virus type-1 non-nucleoside reverse transcriptase inhibitors. *Med Res Rev* 2019;**39**:1235–73.
19. Wu G, Zhao T, Kang D, Zhang J, Song Y, Namasivayam V, et al. Overview of recent strategic advances in medicinal chemistry. *J Med Chem* 2019;**62**:9375–414.
20. Ma Y, Frutos-Beltran E, Kang D, Pannecouque C, De Clercq E, Menendez-Arias L, et al. Medicinal chemistry strategies for discovering antiviral effective against drug-resistant viruses. *Chem Soc Rev* 2021;**50**:4514–40.
21. Lansdon EB, Brendza KM, Hung M, Wang R, Mukund S, Jin D, et al. Crystal structures of HIV-1 reverse transcriptase with etravirine (TMC125) and rilpivirine (TMC278): implications for drug design. *J Med Chem* 2010;**53**:4295–9.
22. Das K, Bauman JD, Clark Jr AD, Frenkel YV, Lewi PJ, Shatkin AJ, et al. High-resolution structures of HIV-1 reverse transcriptase/TMC278 complexes: strategic flexibility explains potency against resistance mutations. *Proc Natl Acad Sci U S A* 2008;**105**:1466–71.
23. Lovering F, Bikker J, Humblet C. Escape from flatland: increasing saturation as an approach to improving clinical success. *J Med Chem* 2009;**52**:6752–6.
24. Wei W, Cherukupalli S, Jing L, Liu X, Zhan P. Fsp<sup>3</sup>: a new parameter for drug-likeness. *Drug Discov Today* 2020;**25**:1839–45.
25. Frey KM, Bollini M, Mislak AC, Cisneros JA, Gallardo-Macias R, Jorgensen WL, et al. Crystal structures of HIV-1 reverse transcriptase with picomolar inhibitors reveal key interactions for drug design. *J Am Chem Soc* 2012;**134**:19501–3.
26. Kudalkar SN, Beloor J, Quijano E, Spasov KA, Lee WG, Cisneros JA, et al. From in silico hit to long-acting late-stage preclinical candidate to combat HIV-1 infection. *Proc Natl Acad Sci U S A* 2018;**115**:E802–E11.
27. Kourounakis AP, Xanthopoulos D, Tzara A. Morpholine as a privileged structure: a review on the medicinal chemistry and pharmacological activity of morpholine containing bioactive molecules. *Med Res Rev* 2020;**40**:709–52.
28. Huang B, Chen W, Zhao T, Li Z, Jiang X, Ginex T, et al. Exploiting the tolerant region I of the non-nucleoside reverse transcriptase inhibitor (NNRTI) binding pocket: discovery of potent diarylpyrimidine-typed HIV-1 NNRTIs against wild-type and E138K mutant virus with significantly improved water solubility and favorable safety profiles. *J Med Chem* 2019;**62**:2083–98.
29. Wang Z, Kang D, Feng D, Cherukupalli S, Jiang X, Fu Z, et al. Targeting dual tolerant regions of binding pocket: discovery of novel morpholine-substituted diarylpyrimidines as potent HIV-1 NNRTIs with significantly improved water solubility. *Eur J Med Chem* 2020;**206**:112811.
30. Kang D, Fang Z, Li Z, Huang B, Zhang H, Lu X, et al. Design, synthesis, and evaluation of thiophene[3,2-*d*]pyrimidine derivatives as HIV-1 non-nucleoside reverse transcriptase inhibitors with significantly improved drug resistance profiles. *J Med Chem* 2016;**59**:7991–8007.
31. Kang D, Fang Z, Huang B, Lu X, Zhang H, Xu H, et al. Structure-based optimization of thiophene[3,2-*d*]pyrimidine derivatives as potent HIV-1 non-nucleoside reverse transcriptase inhibitors with improved potency against resistance-associated variants. *J Med Chem* 2017;**60**:4424–43.
32. Avgy-David HH, Senderowitz H. Toward focusing conformational ensembles on bioactive conformations: a molecular mechanics/quantum mechanics study. *J Chem Inf Model* 2015;**55**:2154–67.
33. Zheng Y, Tice CM, Singh SB. Conformational control in structure-based drug design. *Bioorg Med Chem Lett* 2017;**27**:2825–37.
34. Kuhn B, Guba W, Hert J, Banner D, Bissantz C, Ceccarelli S, et al. A real-world perspective on molecular design. *J Med Chem* 2016;**59**:4087–102.
35. Goto T, Shiina A, Murata T, Tomii M, Yamazaki T, Yoshida K, et al. Identification of the 5,5-dioxo-7,8-dihydro-6*H*-thiopyrano[3,2-*d*]pyrimidine derivatives as highly selective PDE4B inhibitors. *Bioorg Med Chem Lett* 2014;**24**:893–9.
36. Tang G, Kertesz DJ, Yang M, Lin X, Wang Z, Li W, et al. Exploration of piperidine-4-yl-aminopyrimidines as HIV-1 reverse transcriptase inhibitors. N-Phenyl derivatives with broad potency against resistant mutant viruses. *Bioorg Med Chem Lett* 2010;**20**:6020–3.
37. Wang Z, Zalloum WA, Wang W, Jiang X, De Clercq E, Pannecouque C, et al. Discovery of novel dihydrothiopyrano[4,3-*d*]pyrimidine derivatives as potent HIV-1 NNRTIs with significantly reduced hERG inhibitory activity and improved resistance profiles. *J Med Chem* 2021;**64**:13658–75.
38. Melikian GL, Rhee SY, Varghese V, Porter D, White K, Taylor J, et al. Non-nucleoside reverse transcriptase inhibitor (NNRTI) cross-resistance: implications for preclinical evaluation of novel NNRTIs

- and clinical genotypic resistance testing. *J Antimicrob Chemother* 2014;**69**:12–20.
39. Gupta S, Fransen S, Paxinos EE, Stawiski E, Huang W, Petropoulos CJ. Combinations of mutations in the connection domain of human immunodeficiency virus type 1 reverse transcriptase: assessing the impact on nucleoside and nonnucleoside reverse transcriptase inhibitor resistance. *Antimicrob Agents Chemother* 2010;**54**:1973–80.
  40. Rhee SY, Tzou PL, Shafer RW. Temporal trends in HIV-1 mutations used for the surveillance of transmitted drug resistance. *Viruses* 2021;**13**:879.
  41. McClung RP, Oster AM, Ocfemia MCB, Saduvala N, Heneine W, Johnson JA, et al. Transmitted drug resistance among human immunodeficiency virus (HIV)-1 diagnoses in the United States, 2014–2018. *Clin Infect Dis* 2022;**74**:1055–62.
  42. Vingerhoets J, Tambuyzer L, Azijn H, Hoogstoel A, Nijs S, Peeters M, et al. Resistance profile of etravirine: combined analysis of baseline genotypic and phenotypic data from the randomized, controlled Phase III clinical studies. *AIDS* 2010;**24**:503–14.
  43. Gupta S, Vingerhoets J, Fransen S, Tambuyzer L, Azijn H, Frantzell A, et al. Connection domain mutations in HIV-1 reverse transcriptase do not impact etravirine susceptibility and virologic responses to etravirine-containing regimens. *Antimicrob Agents Chemother* 2011;**55**:2872–9.
  44. Reuman EC, Rhee SY, Holmes SP, Shafer RW. Constrained patterns of covariation and clustering of HIV-1 non-nucleoside reverse transcriptase inhibitor resistance mutations. *J Antimicrob Chemother* 2010;**65**:1477–85.
  45. Rimsky L, Vingerhoets J, Van Eygen V, Eron J, Clotet B, Hoogstoel A, et al. Genotypic and phenotypic characterization of HIV-1 isolates obtained from patients on rilpivirine therapy experiencing virologic failure in the phase 3 ECHO and THRIVE studies: 48-week analysis. *J Acquir Immune Defic Syndr* 2012;**59**:39–46.
  46. Xu HT, Colby-Germinario SP, Asahchop EL, Oliveira M, McCallum M, Schader SM, et al. Effect of mutations at position E138 in HIV-1 reverse transcriptase and their interactions with the M184I mutation on defining patterns of resistance to nonnucleoside reverse transcriptase inhibitors rilpivirine and etravirine. *Antimicrob Agents Chemother* 2013;**57**:3100–9.
  47. Smith SJ, Pauly GT, Akram A, Melody K, Ambrose Z, Schneider JP, et al. Rilpivirine and doravirine have complementary efficacies against NNRTI-resistant HIV-1 mutants. *J Acquir Immune Defic Syndr* 2016;**72**:485–91.
  48. Brenner BG, Oliveira M, Ibanescu RI, Routy JP, Thomas R. Cell culture selections reveal favourable drug resistance profiles for doravirine and islatravir. *J Antimicrob Chemother* 2021;**76**:2137–42.
  49. Yang Y, Kang D, Nguyen LA, Smithline ZB, Pannecouque C, Zhan P, et al. Structural basis for potent and broad inhibition of HIV-1 RT by thiophene[3,2-*d*]pyrimidine non-nucleoside inhibitors. *Elife* 2018;**7**:e36340.
  50. Ren J, Nichols CE, Chamberlain PP, Weaver KL, Short SA, Stammers DK. Crystal structures of HIV-1 reverse transcriptases mutated at codons 100, 106 and 108 and mechanisms of resistance to non-nucleoside inhibitors. *J Mol Biol* 2004;**336**:569–78.
  51. Guengerich FP, Waterman MR, Egli M. Recent structural insights into cytochrome P450 function. *Trends Pharmacol Sci* 2016;**37**:625–40.
  52. Havens JP, Podany AT, Scarsi KK, Fletcher CV. Clinical pharmacokinetics and pharmacodynamics of etravirine: an updated review. *Clin Pharmacokinet* 2020;**59**:137–54.
  53. Sharma M, Saravolatz LD. Rilpivirine: a new non-nucleoside reverse transcriptase inhibitor. *J Antimicrob Chemother* 2013;**68**:250–6.
  54. Wang W, MacKinnon R. Cryo-EM structure of the open human ether-à-go-go-related K<sup>+</sup> channel hERG. *Cell* 2017;**169**:422–30.
  55. Hwang C, Lai MT, Hazuda D. Rational design of doravirine: from bench to patients. *ACS Infect Dis* 2020;**6**:64–73.